

A Note on Kinematic Flow and Differential Equations for Two-Site One-Loop Graph in FRW Spacetime

Yanfeng Hang,^a Cong Shen^a

^a*Department of Physics and Astronomy,
Northwestern University, Evanston, IL 60208, USA*

E-mail: yfhang@northwestern.edu, CongShen2028@u.northwestern.edu

ABSTRACT: In this study, we investigate the canonical differential equations governing the two-site one-loop wavefunction coefficient in conformally-coupled scalar theory within a general FRW cosmology. By employing relative twisted cohomology and integration by parts, we systematically derive these equations, providing a solid foundation for further analysis. Notably, we extend the kinematic flow framework to the loop level for the first time, efficiently deriving the differential equations through a graphical approach using family trees generated by tubing graphs, which are associated with the singularities of the system. In addition, we provide a preliminary discussion on higher-loop cases, laying the groundwork for future exploration of more complex scenarios. This methodology offers valuable insights into the dynamical behavior of the differential system for the loop-level cosmological wavefunction coefficient.

arXiv:2410.17192 [hep-th]

Contents

1	Introduction	1
2	Toy Model and Cosmological Wavefunction Coefficients	2
3	Two-Site One-Loop Wavefunction Coefficients and Canonical DEs	5
3.1	Two-Site One-Loop Bubble	5
3.1.1	Hyperplane Arrangements	6
3.1.2	Derivation of Canonical DEs via IBP	9
3.2	Two-Site One-Loop Tadpole	14
3.3	New Features of Hyperplane Arrangement at Loop Level	21
4	Kinematic Flow for Two-Site One-Loop Graph	21
4.1	Two-Site One-Loop Bubble	22
4.2	Two-Site One-Loop Tadpole	28
5	Conclusion and Outlook	32
A	The Derivation of Two-Site One-Loop DEs from IBP	33
A.1	Two-Site One-Loop Bubble	33
A.2	Two-Site One-Loop Tadpole	35
B	Analysis for Two-Site Higher Loop Graph	36

1 Introduction

The study of cosmological dynamics has emerged as a central focus in modern theoretical physics, particularly in understanding the early universe and the mechanisms that shaped its evolution. Among the many toy models, the investigation of wavefunction coefficient for conformally-coupled scalars in power-law Friedmann-Robertson-Walker (FRW) spacetime [1, 2] has proven instrumental in advancing our understanding of cosmological processes. These wavefunction coefficients encapsulate key information about inflationary dynamics and the generation of primordial fluctuations, serving as a bridge between theoretical models and observational cosmology.

In recent years, various innovative methods have been developed to compute and study cosmological correlators, unveiling new mathematical structures and offering deeper insights into the nature of the early universe. Notable approaches include: The framework of the cosmological polytope [1–4], which geometrically encodes the combinatorial and analytic properties of correlators; The techniques based on (dual) twisted cohomology, intersection theory and algebraic geometry [5, 6], which study the differentiation system

of FRW wavefunction coefficients at tree- and loop-level; The kinematic flow method [7, 8], which organizes the differential equations of tree-level FRW correlators based on the hierarchical structure of their singularities represented by tubing graphs.

In this work, we focus on the loop-level wavefunction coefficient in conformally-coupled scalar field theory with non-conformal polynomial interactions in a general power-law FRW universe. We utilize relative twisted cohomology [9–11] alongside the integration-by-parts (IBP) to derive the canonical differential equations (DEs) [12, 13] associated with the wavefunction coefficients of two-site one-loop diagrams. A key component of our study is the application and extension of the kinematic flow framework to loop level for the first time. This powerful methodology enables the systematic prediction of canonical differential equations by representing the singularities of the system as marked tubing graphs [7, 8, 14–16]. These graphs encode the hierarchical relationships among the integrals, forming family trees that organize the system’s structure according to some simple rules. By utilizing this framework, we streamline the derivation of differential equations from the family trees constructed by the tubing graphs. This methodology not only enhances computational efficiency but also provides deeper insights into the interplay between the graphical and analytical structures underlying cosmological wavefunction coefficients.

This paper is organized as follows: In Section 2, we set up the toy model of conformally-coupled scalars in FRW background and provide a brief review of cosmological wavefunction coefficients. In Section 3, we analyze the two-site one-loop FRW wavefunction coefficients by using the framework of relative twisted cohomology and hyperplane arrangements. We conduct a systematic analysis of the canonical forms associated with the integral family, exploring their structure within the bounded chambers. And we also derive the corresponding canonical differential equations for the integral family. The derivation relies on matching residues at different codimension-2 boundaries through IBP techniques. We also demonstrate that at loop level, parent functions are non-unique, with the tadpole system requiring two, unlike the unique parent function at tree level. In Section 4, we present the extension of kinematic flow framework from tree-level to loop-level computations for the first time. Singularities in the differential system are represented as the tubing graphs, establishing a direct correspondence between these graphical structures and the differential equations. Finally, in Section 5, we summarize our results and discuss potential directions for future research. The applications to higher-loop computations and extensions to more general cosmological models are summarized in Appendix.

2 Toy Model and Cosmological Wavefunction Coefficients

We consider the model of conformally-coupled scalar fields with a non-conformal polynomial self-interaction term in a general FRW universe. The action of this theory defined in a $(d + 1)$ -dimensional spacetime can be expressed as follows:

$$S_{\text{FRW}} = - \int d^d x \int_{-\infty}^0 d\eta \sqrt{-g} \left[\frac{1}{2} g^{\alpha\beta} \partial_\alpha \phi \partial_\beta \phi + \left(\frac{d-1}{8d} \right) R \phi^2 + \sum_{m \geq 3} \frac{\lambda_m}{m!} \phi^m \right], \quad (2.1)$$

where the FRW metric is defined as follows:

$$ds^2 = g_{\alpha\beta} dx^\alpha dx^\beta = [a(\eta)]^2 (-d\eta^2 + \delta_{ij} dx^i dx^j). \quad (2.2)$$

In Eq. (2.2), $a(\eta)$ represents the scale factor and the indices $(i, j) = 1, \dots, d$ span the spatial dimensions. Further, by substituting FRW metric (2.2) into Eq. (2.1) and rescaling the scalar field as $\phi \rightarrow [a(\eta)]^{-\Delta} \phi$ with $\Delta = (d-1)/2$, the FRW action (2.1) will reduce to the action of a massless scalar field living in a $(d+1)$ -dimensional Minkowski (flat) spacetime:

$$S_{\text{Mink}} = - \int d^d x \int_{-\infty}^0 d\eta \left[\frac{1}{2} (\partial\phi)^2 + \sum_{m \geq 3} \frac{\lambda_m(\eta)}{m!} \phi^m \right], \quad (2.3)$$

where the time-dependent coupling $\lambda_m(\eta)$ is defined as follows:

$$\lambda_m(\eta) \equiv \lambda_m [a(\eta)]^{2-(m-2)\Delta}. \quad (2.4)$$

Now, we provide a brief review of the cosmological wavefunction coefficients. These coefficients describe the amplitude for different configurations of fields in the early universe and encode crucial information about cosmological fluctuations. It can be derived from the path integral formalism, where the wavefunction $\Psi[\varphi]$ is obtained by summing over all possible field configurations $\varphi(x)$ in a given cosmological background. Specifically, the cosmological wavefunction $\Psi[\varphi]$ can be expressed as a path integral over the field configurations:

$$\Psi[\phi] = \int_{\varphi[-\infty(1-i\epsilon)]=0}^{\varphi(0)=\phi} \mathcal{D}\phi e^{iS[\varphi]}, \quad (2.5)$$

where $S[\varphi]$ is the action of the field φ as given in Eq. (2.3) and the integral is performed over all field configurations. And, the $i\epsilon$ -prescription is crucial for suppressing the negative-frequency component and ensuring that the initial state corresponds to a pure, minimal-energy (Bunch-Davies) vacuum at the early time $\eta \rightarrow -\infty$. Further, $|\Psi[\phi]|^2$ provides the physical meaning of the probability density for spatial field configurations. Thus, the equal-time N -point correlation function for ϕ can be written as:

$$\langle \phi(\mathbf{x}_1) \cdots \phi(\mathbf{x}_N) \rangle = \int \mathcal{D}\phi \phi(\mathbf{x}_1) \cdots \phi(\mathbf{x}_N) |\Psi[\phi]|^2. \quad (2.6)$$

The wavefunction can also be expanded in terms of its coefficients, which are related to cosmological correlation functions. For example, expanding $\Psi[\phi]$ perturbatively gives:

$$\Psi[\phi] = \exp \left\{ - \sum_{N \geq 2} \frac{1}{N!} \int \prod_{i=1}^N \frac{d^d \mathbf{k}_i}{(2\pi)^d} \phi_{\mathbf{k}_i} \left[\psi_n(\{\mathbf{k}_j\}) (2\pi)^d \delta^{(d)} \left(\sum_{\ell=1}^N \mathbf{k}_\ell \right) \right] \right\}, \quad (2.7)$$

where $\psi_n(\{\mathbf{k}_j\})$ are the cosmological wavefunction coefficients, encoding the interactions between N -point fluctuations of the field. The leading term $\psi_2(\mathbf{k}_1, \mathbf{k}_2)$ corresponds to the two-point correlation function, higher-order coefficients, like $\psi_3(\mathbf{k}_1, \mathbf{k}_2, \mathbf{k}_3)$, capture interactions between modes and lead to non-Gaussianities.

The path integral can be performed diagrammatically in the usual way with Feynman graphs. Each diagram corresponds to a specific contribution to the perturbative expansion

of the wavefunction, which can be calculated by using the following Feynman rules: (i). Draw the boundary surface at fixed time $\eta = 0$ where the wavefunction will be computed and draw all diagrams ending on the boundary surface. (ii). Attach a vertex factor iV_v to each bulk interaction, where V_v is defined by the interaction terms in the action. For a scalar field with non-derivative polynomial interactions as given in Eq. (2.3), V_v depends only on the coupling constant. (iii). Assign a bulk-to-boundary propagator, $K(E; \eta)$, to each external line. For a given vertex v , this propagator corresponds to the propagation of a field from a bulk vertex to the late-time boundary, and it takes the form:

$$K_v(E_v; \eta_v) = e^{iE_v \eta_v}, \quad (2.8)$$

where $E_v = \sum_i |\mathbf{k}_i|$ denotes the sum of the energies of all i external legs connected to the vertex v . (iv). Assign a bulk-to-bulk propagator, $G(E; \eta, \eta')$, to each internal line. For an internal line e connecting two vertices, v_e and v'_e , the bulk-to-bulk propagator $G_e(E_e; \eta_{v_e}, \eta_{v'_e})$ describes the propagation of fields between two vertices v_e and v'_e located at different times and it takes the form:

$$G_e(E_e; \eta_{v_e}, \eta_{v'_e}) = \frac{1}{2E_e} \left\{ \exp[-iE_e(\eta_{v_e} - \eta_{v'_e})] \theta(\eta_{v_e} - \eta_{v'_e}) \right. \\ \left. + \exp[-iE_e(\eta_{v'_e} - \eta_{v_e})] \theta(\eta_{v'_e} - \eta_{v_e}) \right. \\ \left. - \exp[iE_e(\eta_{v_e} + \eta_{v'_e})] \right\}, \quad (2.9)$$

where $E_e = |\mathbf{k}_e|$ represent the energy of an internal line e . (v). Integrate over the time insertions of all bulk vertices and any loop momenta¹.

Finally, we assume that the scale factor $a(\eta)$ appearing in the FRW metric (2.2) takes the following power-law form [5, 7, 8]:

$$a(\eta) = \eta^{-1-\varepsilon}, \quad (2.10)$$

where the parameter $\varepsilon = 0, -1, -2, -3$ corresponding to the de Sitter (dS), flat/inflation, radiation- and matter-dominated universe, respectively. Thus, in the case of a power-law form (2.10), we can analyze and compute the wavefunction coefficient. The corresponding Feynman rules need slight modifications, where the bulk-to-boundary propagator (2.8) and bulk-to-bulk propagator (2.9) remain unchanged from their flat-space forms. As for the vertices, the coupling of the non-polynomial interaction term in Eq. (2.1) can be expressed in the energy space via following Mellin transformation:

$$\lambda_N(\eta) = \lambda_N \left(\frac{1}{\eta} \right)^{1+\varepsilon} = \int_0^{\infty(1-i\epsilon)} dx \bar{\lambda}_N(x) e^{ix\eta}, \quad (2.11)$$

where the variable x is of the same order as energy and the energy-dependent coupling constant $\bar{\lambda}_N(x)$ is given by

$$\bar{\lambda}_N(x) = \lambda_N \frac{(-i)^\gamma}{\Gamma(\gamma)} x^{\gamma-1}, \quad \gamma = \frac{1+\varepsilon}{2} [4 - (N-2)(d-1)]. \quad (2.12)$$

¹In this analysis, we focus solely on the wavefunction coefficient at the integrand level, without performing integration over loop momenta.

Further, the $i\epsilon$ -prescription helps to regulate the integral when some $\gamma < 0$.

Therefore, for an N -site L -loop graph with vertex set \mathcal{V} and edge set \mathcal{E} , we can compute its FRW wavefunction coefficient by shifting its flat-space form over the external energies:

$$\psi_{N,\text{FRW}}^{(L)}(X_v, Y_e) = \int_0^\infty \prod_{v \in \mathcal{V}} dx_v \bar{\lambda}_N(x) \psi_{N,\text{Mink}}^{(L)}(X_v + x_v, Y_e), \quad (2.13)$$

where X_v, Y_e are associated with the sum of energies flowing to the late-time boundary from a vertex v and the energies of the internal lines e individually. And the flat-space wavefunction coefficient integrand $\psi_{N,\text{Mink}}^{(L)}$ is given by

$$\psi_{N,\text{Mink}}^{(L)}(X_v, Y_e) = i^N \int_{-\infty}^0 \prod_{v \in \mathcal{V}} d\eta_v K_v(X_v; \eta_v) \prod_{e \in \mathcal{E}} G_e(Y_e; \eta_{v_e}, \eta_{v_e^0}), \quad (2.14)$$

where the propagators K_v and G_e are defined in Eqs. (2.8)-(2.9).

3 Two-Site One-Loop Wavefunction Coefficients and Canonical DEs

In this section, we investigate a detailed analysis of the two-site one-loop wavefunction coefficients for bubble and tadpole diagrams within a $(d+1)$ -dimensional power-law FRW universe. For the first time, we systematically find the corresponding integral basis associated with the loop-level wavefunction coefficients guided by the structure of the hyperplane arrangements. Further, we also provide the comprehensive derivations for the canonical differential equations, employing integration-by-parts (IBP) techniques to capture their intricate dependencies.

3.1 Two-Site One-Loop Bubble

We first consider the two-site one-loop bubble-type wavefunction coefficient whose Feynman diagram is shown in Fig. 1. Then, following the Feynman rules given in Section 2, we can compute the flat-space wavefunction coefficient as follows:

$$\psi_{2,\text{Mink}}^{(1)\text{bub}} = i^2 \int_{-\infty}^0 d\eta_1 \int_{-\infty}^0 d\eta_2 K(X_1; \eta_1) K(X_2; \eta_2) G(Y_1; \eta_1, \eta_2) G(Y_2; \eta_2, \eta_1)$$

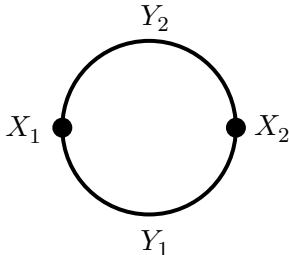


Figure 1. The Feynman diagram for the two-site one-loop bubble wavefunction coefficient, where $\{X_1, X_2\}$ are associated with the sum of energies flowing from the vertices to the late-time boundary (which is omitted in the figure) and $\{Y_1, Y_2\}$ represent the energies of the internal lines.

$$= \frac{2(X_1+X_2+Y_1+Y_2)}{(X_1+X_2)(X_1+X_2+2Y_1)(X_1+X_2+2Y_2)(X_1+Y_1+Y_2)(X_2+Y_1+Y_2)}, \quad (3.1)$$

where we have set the coupling $\bar{\lambda} = 1$. Subsequently, to derive the two-site one-loop wavefunction coefficient in a general FRW universe, we start by modifying its corresponding flat-space form (3.1), where this can be achieved by shifting over the external energies of Eq. (3.1) via the transformations: $(X_1, X_2) \rightarrow (X_1+x_1, X_2+x_2)$. Then, we also incorporate a twist term $(x_1x_2)^\varepsilon$ to regularize the integrand, effectively controlling the behavior near singularities through the parameter ε . Therefore, the FRW wavefunction coefficient for two-site one-loop bubble diagram is derived in the following integration representation:

$$\psi_{2,\text{FRW}}^{(1)\text{bub}} = 4Y_1Y_2 \int dx_1 \wedge dx_2 (x_1x_2)^\varepsilon \psi_{2,\text{Mink}}^{(1)\text{bub}} \Big|_{X_2 \rightarrow X_2+x_2}^{X_1 \rightarrow X_1+x_1}, \quad (3.2)$$

where we have also included an overall factor of $4Y_1Y_2$ for later convenience.

3.1.1 Hyperplane Arrangements

Although it is possible to directly compute the integrals in Eq. (3.2), there are more efficient and elegant approaches to tackle it. Therefore, we will adopt concepts from intersection theory [9–11] combined with the method of canonical differential equations [12, 13] to evaluate the Eq. (3.2). Thus, we can rewrite two-site one-loop FRW correlator (3.2) as:

$$\psi_{2,\text{FRW}}^{(1)\text{bub}} \equiv \int (T_1T_2)^\varepsilon \Omega_{\mathcal{P}}^2 = \int dx_1 \wedge dx_2 (T_1T_2)^\varepsilon \left[\frac{4Y_1Y_2}{L_1L_2D_3} \left(\frac{1}{D_1} + \frac{1}{D_2} \right) \right]. \quad (3.3)$$

In Eq. (3.3), we have defined:

$$\begin{aligned} T_1 &= x_1, & T_2 &= x_2, \\ L_1 &= x_1+X_1+Y_1+Y_2, & L_2 &= x_2+X_2+Y_1+Y_2, \\ D_1 &= x_1+x_2+X_1+X_2+2Y_1, & D_2 &= x_1+x_2+X_1+X_2+2Y_2, \\ D_3 &= x_1+x_2+X_1+X_2, \end{aligned} \quad (3.4)$$

where those divisors are expressed in the linear form, corresponding to seven hyperplanes determined by the equations: $\{T_i, L_j, D_k\} = 0$. Their geometric arrangement in the (x_1, x_2) -coordinate system is illustrated in Fig. 2. Inspecting Eq. (3.3), the extra normalization factor of $4Y_1Y_2$ is included in order to ensure that the canonical 2-form $\Omega_{\mathcal{P}}^2$ has the residues of ± 1 on all codimension-2 boundaries [17]. Moreover, the branch planes $\{T_1, T_2\}$ represent the twisted singularities within the integrand, regulated by the parameter ε , while the hyperplanes $\{L_i, D_j\}$ correspond to the relative singularities. The overall analytic structure of these integrals is fundamentally governed by the intersections of the surfaces $\{T_i, L_j, D_k\}$, as these intersections dictate the behavior and singularities of the whole system.

As discussed in Refs. [9–11], the number of independent master integrals is equal to the number of chambers bounded by the hyperplanes (3.4). For the first time, our detailed analysis reveals that Fig. 2 can be partitioned into three distinct subsystems of hyperplane arrangements. Each subsystem shares four common hyperplanes $\{T_1, T_2, L_1, L_2\}$, while each

subsystem contains a unique diagonally-placed hyperplanes $\{D_1, D_2, D_3\}$. Consequently, Fig. 2 encompasses a total of twelve bounded chambers. These bounded chambers correspond to canonical forms, represented as triangles formed through the intersection of hyperplanes, as established in the framework of Ref. [17]. Based on this foundation, Refs. [7, 8] demonstrate that each chamber uniquely maps to a specific wavefunction coefficient. Therefore, within each subsystem of hyperplanes, there exists a hierarchical structure of functions comprising a “parent” function \mathcal{P}_i accompanied by three “decedent” functions: $\mathcal{F}_i, \tilde{\mathcal{F}}_i$ and \mathcal{Q}_i . These twelve functions collectively form three sets:

$$\mathbf{F}_i \equiv \{ \mathcal{P}_i, \mathcal{F}_i, \tilde{\mathcal{F}}_i, \mathcal{Q}_i \}, \quad i = 1, 2, 3, \quad (3.5)$$

where each function is associated with a bounded triangle region, which is systematically defined as follows:

$$\text{Layer-0: } \triangle_{L_1 L_2 D_i} \leftrightarrow \mathcal{P}_i = \int (T_1 T_2)^\varepsilon \left(\text{dlog} \frac{L_1}{D_i} \wedge \text{dlog} \frac{L_2}{D_i} \right) \equiv \int d\mu \bar{\Omega}_{\mathcal{P}_i}^2, \quad (3.6a)$$

$$\text{Layer-1: } \triangle_{T_1 L_2 D_i} \leftrightarrow \mathcal{F}_i = \int (T_1 T_2)^\varepsilon \left(\text{dlog} \frac{T_1}{D_i} \wedge \text{dlog} \frac{L_2}{D_i} \right) \equiv \int d\mu \bar{\Omega}_{\mathcal{F}_i}^2, \quad (3.6b)$$

$$\triangle_{T_2 L_1 D_i} \leftrightarrow \tilde{\mathcal{F}}_i = \int (T_1 T_2)^\varepsilon \left(\text{dlog} \frac{L_1}{D_i} \wedge \text{dlog} \frac{T_2}{D_i} \right) \equiv \int d\mu \bar{\Omega}_{\tilde{\mathcal{F}}_i}^2, \quad (3.6c)$$

$$\text{Layer-2: } \triangle_{T_1 T_2 D_i} \leftrightarrow \mathcal{Q}_i = \int (T_1 T_2)^\varepsilon \left(\text{dlog} \frac{T_1}{D_i} \wedge \text{dlog} \frac{T_2}{D_i} \right) \equiv \int d\mu \bar{\Omega}_{\mathcal{Q}_i}^2. \quad (3.6d)$$

where $i = \{1, 2, 3\}$. Besides, in Eq. (3.6), we have also re-defined the canonical form as: $\Omega^2 \equiv \bar{\Omega}^2 dx_1 \wedge dx_2$, where $dx_1 \wedge dx_2$ has been further combined with the prefactor $(T_1 T_2)^\varepsilon$ into a compact measure defined as: $d\mu \equiv (T_1 T_2)^\varepsilon dx_1 \wedge dx_2$. To avoid confusion, we will hereafter refer to $\bar{\Omega}$ as the canonical (differential) form. Then, we derive those canonical

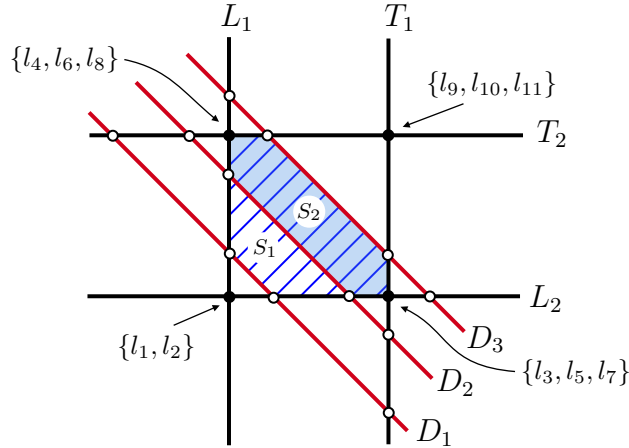


Figure 2. The hyperplane arrangement associated with the two-site one-loop wavefunction coefficient. All the black and white intersection points represent the codimension-2 boundaries. Among these, the four intersection points of L_1, L_2 and T_1, T_2 are used to calculate the letters $\{l_i\}$ in our chosen basis.

forms as follows:

$$\text{Layer-0: } \bar{\Omega}_{\mathcal{P}_1}^2 = \frac{-2Y_2}{L_1 L_2 D_1}, \quad \bar{\Omega}_{\mathcal{P}_2}^2 = \frac{-2Y_1}{L_1 L_2 D_2}, \quad \bar{\Omega}_{\mathcal{P}_3}^2 = \frac{-2(Y_1+Y_2)}{L_1 L_2 D_3}, \quad (3.7a)$$

$$\text{Layer-1: } \bar{\Omega}_{\mathcal{F}_1}^2 = \frac{X_1+Y_1-Y_2}{T_1 L_2 D_1}, \quad \bar{\Omega}_{\mathcal{F}_2}^2 = \frac{X_1-Y_1+Y_2}{T_1 L_2 D_2}, \quad \bar{\Omega}_{\mathcal{F}_3}^2 = \frac{X_1-Y_1-Y_2}{T_1 L_2 D_3}, \quad (3.7b)$$

$$\bar{\Omega}_{\tilde{\mathcal{F}}_1}^2 = \frac{X_2+Y_1-Y_2}{T_2 L_1 D_1}, \quad \bar{\Omega}_{\tilde{\mathcal{F}}_2}^2 = \frac{X_2-Y_1+Y_2}{T_2 L_1 D_2}, \quad \bar{\Omega}_{\tilde{\mathcal{F}}_3}^2 = \frac{X_2-Y_1-Y_2}{T_2 L_1 D_3}, \quad (3.7c)$$

$$\text{Layer-2: } \bar{\Omega}_{\mathcal{Q}_1}^2 = \frac{X_1+X_2+2Y_1}{T_1 T_2 D_1}, \quad \bar{\Omega}_{\mathcal{Q}_2}^2 = \frac{X_1+X_2+2Y_2}{T_1 T_2 D_2}, \quad \bar{\Omega}_{\mathcal{Q}_3}^2 = \frac{X_1+X_2}{T_1 T_2 D_3}. \quad (3.7d)$$

Specifically, we define canonical forms with a positively oriented convention, ensuring that the aforementioned $\bar{\Omega}$ are positive within the corresponding bounded region. In Eqs. (3.6)-(3.7), we have categorized functions/forms into three layers:

- Layer-0: The functions in this layer $\{\mathcal{P}_i\}$ do not involve the twist planes T_1 and T_2 .
- Layer-1: The functions in this layer are obtained by replacing L_1 and L_2 plane in the corresponding Layer-0 function with a twist plane T_1 and T_2 individually i.e., $\mathcal{F}_i = \mathcal{P}_i(L_1 \rightarrow T_1)$ $\tilde{\mathcal{F}}_i = \mathcal{P}_i(L_2 \rightarrow T_2)$.
- Layer-2: The functions in this layer are derived by further replacing the remaining L_1 or L_2 plane in the corresponding Layer-1 functions with a twist plane T_1 or T_2 i.e., $\mathcal{Q}_i = \mathcal{F}_i(L_2 \rightarrow T_2) = \tilde{\mathcal{F}}_i(L_1 \rightarrow T_1)$.

Further, each set \mathbf{F}_i in Eq. (3.5) contains four members, each corresponding to a canonical 2-form uniquely associated with a codimension-2 boundary, represented by the four black intersection points shown in Fig. 2. Thus, for each set of \mathbf{F}_i , any form can be decomposed into this basis by matching residues at these distinctive points, which correspond to the dlog singularities of the form.

However, analyzing the hyperplane arrangement reveals that the twelve chambers (triangles) are not independent, they are subject to two linear constraints, which can be expressed as follows:

$$\begin{aligned} S_1 &= \Delta_{T_1 T_2 D_1} - \Delta_{L_1 T_2 D_1} - \Delta_{L_2 T_1 D_1} - \Delta_{T_1 T_2 D_3} \\ &= \Delta_{L_1 L_2 D_3} - \Delta_{L_1 T_2 D_3} - \Delta_{L_2 T_1 D_3} - \Delta_{L_1 L_2 D_1}, \end{aligned} \quad (3.8a)$$

$$\begin{aligned} S_2 &= \Delta_{T_1 T_2 D_2} - \Delta_{L_1 T_2 D_2} - \Delta_{L_2 T_1 D_2} - \Delta_{T_1 T_2 D_3} \\ &= \Delta_{L_1 L_2 D_3} - \Delta_{L_1 T_2 D_3} - \Delta_{L_2 T_1 D_3} - \Delta_{L_1 L_2 D_2}, \end{aligned} \quad (3.8b)$$

where S_1 and S_2 are correspond to the blue-shaded and blue hexagonal regions in Fig. 2, respectively. Each region can be constructed by stitching together several triangles defined earlier, with two distinct ways of assembling them. Hence, with consistent choice of orientation the constraints (3.8) induce two linear relations among the canonical forms:

$$\bar{\Omega}_{\mathcal{Q}_1}^2 - \bar{\Omega}_{\tilde{\mathcal{F}}_1}^2 - \bar{\Omega}_{\mathcal{F}_1}^2 - \bar{\Omega}_{\mathcal{Q}_3}^2 = \bar{\Omega}_{\mathcal{P}_3}^2 - \bar{\Omega}_{\tilde{\mathcal{F}}_3}^2 - \bar{\Omega}_{\mathcal{F}_3}^2 - \bar{\Omega}_{\mathcal{P}_1}^2, \quad (3.9a)$$

$$\bar{\Omega}_{\mathcal{Q}_2}^2 - \bar{\Omega}_{\tilde{\mathcal{F}}_2}^2 - \bar{\Omega}_{\mathcal{F}_2}^2 - \bar{\Omega}_{\mathcal{Q}_3}^2 = \bar{\Omega}_{\mathcal{P}_3}^2 - \bar{\Omega}_{\tilde{\mathcal{F}}_3}^2 - \bar{\Omega}_{\mathcal{F}_3}^2 - \bar{\Omega}_{\mathcal{P}_2}^2. \quad (3.9b)$$

where these conditions reduce the total member of our chosen basis from twelve to ten. Given our focus on the original form $\bar{\Omega}_{\mathcal{P}}^2$ in Eq. (3.3), we find that the forms $\{\bar{\Omega}_{\mathcal{P}_i}^2\}$ in Eq. (3.6a) can be combined through the following linear superposition:

$$\bar{\Omega}_{\mathcal{P}}^2 = \bar{\Omega}_{\mathcal{P}_1}^2 + \bar{\Omega}_{\mathcal{P}_2}^2 - \bar{\Omega}_{\mathcal{P}_3}^2, \quad (3.10)$$

where we can select \mathcal{P} as an independent basis element instead of $\{\mathcal{P}_i\}$.

Therefore, the ten independent members of our chosen basis belong to the following integral family:

$$\mathbf{I} = (\mathcal{P}, \mathcal{F}_1, \mathcal{F}_2, \mathcal{F}_3, \tilde{\mathcal{F}}_1, \tilde{\mathcal{F}}_2, \tilde{\mathcal{F}}_3, \mathcal{Q}_1, \mathcal{Q}_2, \mathcal{Q}_3)^T. \quad (3.11)$$

Indeed, the canonical forms associated with the bounded chambers naturally provide an “ ε -form” [12, 13] basis for this integral family \mathbf{I} , where each integral has uniform transcendental weight (UT). Hence, \mathbf{I} satisfies a linear system of differential equations in a simple canonical form, governed by a first-order equation:

$$d\mathbf{I}(\mathbf{z}, \varepsilon) = \varepsilon \tilde{A}(\mathbf{z}) \mathbf{I}(\mathbf{z}, \varepsilon), \quad (3.12)$$

where $\mathbf{z} = \{X_1, X_2, Y_1, Y_2\}$ is the set of independent kinematic variables. And the matrix \tilde{A} has the dlog form:

$$\tilde{A}(\mathbf{z}) = \sum_i c_i d\log[w_i(\mathbf{z})] \equiv \sum_i c_i l_i, \quad (3.13)$$

where the matrix \tilde{A} obeys the following integrability conditions:

$$d\tilde{A} = 0, \quad \tilde{A} \wedge \tilde{A} = 0. \quad (3.14)$$

Further, in the above expression (3.13), $\{c_i\}$ are the constant matrices and $\{w_i\}$ represent the “(symbol) letters” [18, 19] which are the rational or algebraic functions of kinematic variables, and the set of all letters are called the “alphabet”. For convenience, we have also defined the dlog form of w_i as l_i in Eq. (3.13). In the subsequent discussion, we will refer to l_i as a letter and the complete set of all independent l_i as the alphabet.

3.1.2 Derivation of Canonical DEs via IBP

In this section, let us calculate the differential equations (3.12) by using the approach of integration-by-parts (IBP). We start by considering $\mathbf{F}_1 = \{\mathcal{P}_1, \mathcal{F}_1, \tilde{\mathcal{F}}_1, \mathcal{Q}_1\}$ where the total derivative for \mathbf{F}_1 is given by

$$d\mathbf{F}_1 = \partial_{X_1} \mathbf{F}_1 dX_1 + \partial_{X_2} \mathbf{F}_1 dX_2 + \partial_{Y_1} \mathbf{F}_1 dY_1 + \partial_{Y_2} \mathbf{F}_1 dY_2. \quad (3.15)$$

For the parent function \mathcal{P}_1 , the differentiation of \mathcal{P}_1 with respect to external energy X_1 is equal to the derivative with respect to x_1 . Thus, we can compute

$$\partial_{X_1} \mathcal{P}_1 = \int d\mu \partial_{x_1} \bar{\Omega}_{\mathcal{P}_1}^2 = \varepsilon \int d\mu \left(-\frac{\bar{\Omega}_{\mathcal{P}_1}^2}{T_1} \right)$$

$$\begin{aligned}
&= \varepsilon \int d\mu \left\{ \left(\text{Res} \left[\frac{-\bar{\Omega}_{\mathcal{P}_1}^2}{T_1} \right]_{\substack{L_1=0 \\ L_2=0}}, \text{Res} \left[\frac{-\bar{\Omega}_{\mathcal{P}_1}^2}{T_1} \right]_{\substack{T_1=0 \\ L_2=0}} \right) (\bar{\Omega}_{\mathcal{P}_1}^2, \bar{\Omega}_{\mathcal{F}_1}^2)^T \right\} \\
&= \varepsilon \int d\mu \left[\frac{1}{X_1+Y_1+Y_2} \bar{\Omega}_{\mathcal{P}_1}^2 + \frac{2Y_2}{(X_1+Y_1-Y_2)(X_1+Y_1+Y_2)} \bar{\Omega}_{\mathcal{F}_1}^2 \right] \\
&= \varepsilon \left[\frac{1}{X_1+Y_1+Y_2} \mathcal{P}_1 + \left(\frac{1}{X_1+Y_1-Y_2} - \frac{1}{X_1+Y_1+Y_2} \right) \mathcal{F}_1 \right]. \tag{3.16}
\end{aligned}$$

Similarly, the differentiation of \mathcal{P}_1 with respect to X_2 proceeds analogously to that of X_1 . We simply need to replace $X_1 \rightarrow X_2$ and $\mathcal{F}_1 \rightarrow \tilde{\mathcal{F}}_1$ in Eq. (3.16) and obtain

$$\partial_{X_2} \mathcal{P}_1 = \varepsilon \left[\frac{1}{X_2+Y_1+Y_2} \mathcal{P}_1 + \left(\frac{1}{X_2+Y_1-Y_2} - \frac{1}{X_2+Y_1+Y_2} \right) \tilde{\mathcal{F}}_1 \right]. \tag{3.17}$$

The calculation of differentiation of \mathcal{P}_1 with respect to the internal energies Y_1 and Y_2 is non-trivial. However, these derivatives can be intuitively computed, yielding the following relations:

$$\begin{aligned}
\partial_{Y_1} \mathcal{P}_1 &= \int d\mu (\partial_{x_1} \bar{\Omega}_{\mathcal{P}_1}^2 + \partial_{x_2} \bar{\Omega}_{\mathcal{P}_1}^2) \\
&= \varepsilon \left[\left(\frac{1}{X_1+Y_1+Y_2} + \frac{1}{X_2+Y_1+Y_2} \right) \mathcal{P}_1 + \left(\frac{1}{X_1+Y_1-Y_2} - \frac{1}{X_1+Y_1+Y_2} \right) \mathcal{F}_1 \right. \\
&\quad \left. + \left(\frac{1}{X_2+Y_1-Y_2} - \frac{1}{X_2+Y_1+Y_2} \right) \tilde{\mathcal{F}}_1 \right], \tag{3.18a}
\end{aligned}$$

$$\begin{aligned}
\partial_{Y_2} \mathcal{P}_1 &= \int d\mu \left[\partial_{x_1} \left(\frac{-x_1 - X_1 - Y_1}{Y_2} \bar{\Omega}_{\mathcal{P}_1}^2 \right) + \partial_{x_2} \left(\frac{-x_2 - X_2 - Y_2}{Y_1} \bar{\Omega}_{\mathcal{P}_1}^2 \right) \right] \\
&= \varepsilon \left[\left(\frac{1}{X_1+Y_1+Y_2} + \frac{1}{X_2+Y_1+Y_2} \right) \mathcal{P}_1 - \left(\frac{1}{X_1+Y_1-Y_2} + \frac{1}{X_1+Y_1+Y_2} \right) \mathcal{F}_1 \right. \\
&\quad \left. - \left(\frac{1}{X_2+Y_1-Y_2} + \frac{1}{X_2+Y_1+Y_2} \right) \tilde{\mathcal{F}}_1 \right]. \tag{3.18b}
\end{aligned}$$

In terms of total derivative (3.19) and expressing in dlog forms, we finally obtain the differential equation for \mathcal{P}_1 as:

$$\begin{aligned}
d\mathcal{P}_1 &= \varepsilon \left[(\mathcal{P}_1 - \mathcal{F}_1) d\log(X_1+Y_1+Y_2) + (\mathcal{P}_1 - \tilde{\mathcal{F}}_1) d\log(X_2+Y_1+Y_2) \right. \\
&\quad \left. + \mathcal{F}_1 d\log(X_1+Y_1-Y_2) + \tilde{\mathcal{F}}_1 d\log(X_2+Y_1-Y_2) \right]. \tag{3.19}
\end{aligned}$$

Next, we examine the differentiation of the decedent functions $\mathcal{F}_1, \tilde{\mathcal{F}}_1$ and \mathcal{Q}_1 . For \mathcal{F}_1 , the differential results with respect to external energies are computed as:

$$\begin{aligned}
\partial_{X_1} \mathcal{F}_1 &= \int d\mu \left[\partial_{x_1} \left(\frac{-T_1}{X_1+Y_1-Y_2} \bar{\Omega}_{\mathcal{F}_1}^2 \right) + \partial_{x_2} \left(\frac{-L_2}{X_1+Y_1-Y_2} \bar{\Omega}_{\mathcal{F}_1}^2 \right) \right] \\
&= \varepsilon \int d\mu \left\{ \left(\text{Res} \left[\frac{\bar{\Omega}_{\mathcal{F}_1}^2}{X_1+Y_1-Y_2} \right]_{\substack{T_1=0 \\ L_2=0}}, \text{Res} \left[\frac{\bar{\Omega}_{\mathcal{F}_1}^2}{X_1+Y_1-Y_2} \right]_{\substack{T_1=0 \\ T_2=0}} \right) (\bar{\Omega}_{\mathcal{F}_1}^2, \bar{\Omega}_{\mathcal{Q}_1}^2)^T \right. \\
&\quad \left. + \left(\text{Res} \left[\frac{L_2 \bar{\Omega}_{\mathcal{F}_1}^2}{T_2(X_1+Y_1-Y_2)} \right]_{\substack{T_1=0 \\ L_2=0}}, \text{Res} \left[\frac{L_2 \bar{\Omega}_{\mathcal{F}_1}^2}{T_2(X_1+Y_1-Y_2)} \right]_{\substack{T_1=0 \\ T_2=0}} \right) (\bar{\Omega}_{\mathcal{F}_1}^2, \bar{\Omega}_{\mathcal{Q}_1}^2)^T \right\}
\end{aligned}$$

$$= \varepsilon \left[\frac{1}{X_1+Y_1-Y_2} \mathcal{F}_1 + \frac{1}{X_1+X_2+2Y_1} \mathcal{Q}_1 \right], \quad (3.20a)$$

$$\begin{aligned} \partial_{X_2} \mathcal{F}_1 &= \int d\mu \partial_{x_2} \bar{\Omega}_{\mathcal{F}_1}^2 \\ &= \varepsilon \left[\frac{1}{X_2+Y_1+Y_2} \mathcal{F}_1 + \left(\frac{1}{X_1+X_2+2Y_1} - \frac{1}{X_2+Y_1+Y_2} \right) \mathcal{Q}_1 \right], \end{aligned} \quad (3.20b)$$

and the results for differentiation with respect to the internal energies are

$$\begin{aligned} \partial_{Y_1} \mathcal{F}_1 &= \int d\mu \left[\partial_{x_1} \left(\frac{-T_1}{X_1+Y_1-Y_2} \bar{\Omega}_{\mathcal{F}_1}^2 \right) + \partial_{x_2} \left(\frac{-T_1-2L_2+D_1}{X_1+Y_1-Y_2} \bar{\Omega}_{\mathcal{F}_1}^2 \right) \right] \\ &= \varepsilon \left[\left(\frac{1}{X_1+Y_1-Y_2} + \frac{1}{X_2+Y_1+Y_2} \right) \mathcal{F}_1 + \left(\frac{2}{X_1+X_2+2Y_1} - \frac{1}{X_2+Y_1+Y_2} \right) \mathcal{Q}_1 \right], \end{aligned} \quad (3.21a)$$

$$\begin{aligned} \partial_{Y_2} \mathcal{F}_1 &= \int d\mu \left[\partial_{x_1} \left(\frac{T_1}{X_1+Y_1-Y_2} \bar{\Omega}_{\mathcal{F}_1}^2 \right) + \partial_{x_2} \left(\frac{-T_1+D_1}{X_1+Y_1-Y_2} \bar{\Omega}_{\mathcal{F}_1}^2 \right) \right] \\ &= \varepsilon \left[\left(-\frac{1}{X_1+Y_1-Y_2} + \frac{1}{X_2+Y_1+Y_2} \right) \mathcal{F}_1 - \frac{1}{X_2+Y_1+Y_2} \mathcal{Q}_1 \right]. \end{aligned} \quad (3.21b)$$

The calculation for $\tilde{\mathcal{F}}_1$ is similar to that of \mathcal{F}_1 , we will not provide the details. Thus, in terms of total derivative, we can obtain the following differential equations for \mathcal{F}_1 and $\tilde{\mathcal{F}}_1$:

$$\begin{aligned} d\mathcal{F}_1 &= \varepsilon [\mathcal{F}_1 d\log(X_1+Y_1-Y_2) + (\mathcal{F}_1 - \mathcal{Q}_1) d\log(X_2+Y_1+Y_2) \\ &\quad + \mathcal{Q}_1 d\log(X_1+X_2+2Y_1)], \end{aligned} \quad (3.22a)$$

$$\begin{aligned} d\tilde{\mathcal{F}}_1 &= \varepsilon [\tilde{\mathcal{F}}_1 d\log(X_2+Y_1-Y_2) + (\tilde{\mathcal{F}}_1 - \mathcal{Q}_1) d\log(X_1+Y_1+Y_2) \\ &\quad + \mathcal{Q}_1 d\log(X_1+X_2+2Y_1)]. \end{aligned} \quad (3.22b)$$

Finally, for \mathcal{Q}_1 , we can derive

$$\begin{aligned} \partial_{X_1} \mathcal{Q}_1 &= \int d\mu \left[\partial_{x_1} \left(\frac{-T_1}{X_1+X_2+2Y_1} \bar{\Omega}_{\mathcal{Q}_1}^2 \right) + \partial_{x_2} \left(\frac{-T_2}{X_1+X_2+2Y_1} \bar{\Omega}_{\mathcal{Q}_1}^2 \right) \right] \\ &= 2\varepsilon \int d\mu \left(\text{Res} \left[\frac{\bar{\Omega}_{\mathcal{Q}_1}^2}{X_1+X_2+2Y_1} \right]_{\substack{T_1=0 \\ T_2=0}} \bar{\Omega}_{\mathcal{Q}_1}^2 \right) = 2\varepsilon \left(\frac{1}{X_1+X_2+2Y_1} \right) \mathcal{Q}_1, \end{aligned} \quad (3.23a)$$

$$\partial_{X_2} \mathcal{Q}_1 = \partial_{X_1} \mathcal{Q}_1 = 2\varepsilon \left(\frac{1}{X_1+X_2+2Y_1} \right) \mathcal{Q}_1, \quad (3.23b)$$

$$\begin{aligned} \partial_{Y_1} \mathcal{Q}_1 &= \int d\mu \left[\partial_{x_1} \left(\frac{-2T_1}{X_1+X_2+2Y_1} \bar{\Omega}_{\mathcal{Q}_1}^2 \right) + \partial_{x_2} \left(\frac{-2T_2}{X_1+X_2+2Y_1} \bar{\Omega}_{\mathcal{Q}_1}^2 \right) \right] \\ &= \frac{4\varepsilon}{X_1+X_2+2Y_1} \mathcal{Q}_1, \end{aligned} \quad (3.23c)$$

$$\partial_{Y_2} \mathcal{Q}_1 = 0. \quad (3.23d)$$

Therefore, the differential equation for \mathcal{Q}_1 is given by

$$d\mathcal{Q}_1 = 2\varepsilon \mathcal{Q}_1 d\log(X_1+X_2+2Y_1). \quad (3.24)$$

The differential equations for $\mathbf{F}_2 = \{\mathcal{P}_2, \mathcal{F}_2, \tilde{\mathcal{F}}_2, \mathcal{Q}_2\}$ can be directly derived from those of \mathbf{F}_1 by substituting $Y_1 \rightarrow Y_2$ in the dlog forms and relabeling the function subscripts $1 \rightarrow 2$. The resulting equations are summarized as follows:

$$\begin{aligned} d\mathcal{P}_2 = \varepsilon [& (\mathcal{P}_2 - \mathcal{F}_2) \text{dlog}(X_1 + Y_1 + Y_2) + (\mathcal{P}_2 - \tilde{\mathcal{F}}_2) \text{dlog}(X_2 + Y_1 + Y_2) \\ & + \mathcal{F}_2 \text{dlog}(X_1 - Y_1 + Y_2) + \tilde{\mathcal{F}}_2 \text{dlog}(X_2 - Y_1 + Y_2)], \end{aligned} \quad (3.25a)$$

$$\begin{aligned} d\mathcal{F}_2 = \varepsilon [& \mathcal{F}_2 \text{dlog}(X_1 - Y_1 + Y_2) + (\mathcal{F}_2 - \mathcal{Q}_2) \text{dlog}(X_2 + Y_1 + Y_2) \\ & + \mathcal{Q}_2 \text{dlog}(X_1 + X_2 + 2Y_2)], \end{aligned} \quad (3.25b)$$

$$\begin{aligned} d\tilde{\mathcal{F}}_2 = \varepsilon [& \tilde{\mathcal{F}}_2 \text{dlog}(X_2 - Y_1 + Y_2) + (\tilde{\mathcal{F}}_2 - \mathcal{Q}_2) \text{dlog}(X_1 + Y_1 + Y_2) \\ & + \mathcal{Q}_2 \text{dlog}(X_2 + X_2 + 2Y_2)], \end{aligned} \quad (3.25c)$$

$$d\mathcal{Q}_2 = 2\varepsilon \mathcal{Q}_2 \text{dlog}(X_1 + X_2 + 2Y_2). \quad (3.25d)$$

In Appendix A.1, we provide the derivation of the DEs for $\mathbf{F}_3 = \{\mathcal{P}_3, \mathcal{F}_3, \tilde{\mathcal{F}}_3, \mathcal{Q}_3\}$, the results are summarized as:

$$\begin{aligned} d\mathcal{P}_3 = \varepsilon [& (\mathcal{P}_3 - \mathcal{F}_3) \text{dlog}(X_1 + Y_1 + Y_2) + (\mathcal{P}_3 - \tilde{\mathcal{F}}_3) \text{dlog}(X_2 + Y_1 + Y_2) \\ & + \mathcal{F}_3 \text{dlog}(X_1 - Y_1 - Y_2) + \tilde{\mathcal{F}}_3 \text{dlog}(X_2 - Y_1 - Y_2)], \end{aligned} \quad (3.26a)$$

$$d\mathcal{F}_3 = \varepsilon [\mathcal{F}_3 \text{dlog}(X_1 - Y_1 - Y_2) + (\mathcal{F}_3 - \mathcal{Q}_3) \text{dlog}(X_2 + Y_1 + Y_2) + \mathcal{Q}_3 \text{dlog}(X_1 + X_2)], \quad (3.26b)$$

$$d\tilde{\mathcal{F}}_3 = \varepsilon [\tilde{\mathcal{F}}_3 \text{dlog}(X_2 - Y_1 - Y_2) + (\tilde{\mathcal{F}}_3 - \mathcal{Q}_3) \text{dlog}(X_1 + Y_1 + Y_2) + \mathcal{Q}_3 \text{dlog}(X_1 + X_2)], \quad (3.26c)$$

$$d\mathcal{Q}_3 = 2\varepsilon \mathcal{Q}_3 \text{dlog}(X_1 + X_2). \quad (3.26d)$$

In addition, based on Eq. (3.10), we combine Eq. (3.19), Eq. (3.25a) with Eq. (3.26a) to derive the final differential equation for \mathcal{P} :

$$\begin{aligned} d\mathcal{P} = \varepsilon [& \left(\mathcal{P} - \sum_{i=1}^3 \mathcal{F}_i \right) \text{dlog}(X_1 + Y_1 + Y_2) + \left(\mathcal{P} - \sum_{i=1}^3 \tilde{\mathcal{F}}_i \right) \text{dlog}(X_2 + Y_1 + Y_2) \\ & + \mathcal{F}_1 \text{dlog}(X_1 + Y_1 - Y_2) + \tilde{\mathcal{F}}_1 \text{dlog}(X_2 + Y_1 - Y_2) + \mathcal{F}_2 \text{dlog}(X_1 - Y_1 + Y_2) \\ & + \tilde{\mathcal{F}}_2 \text{dlog}(X_2 - Y_1 + Y_2) + \mathcal{F}_3 \text{dlog}(X_1 - Y_1 - Y_2) + \tilde{\mathcal{F}}_3 \text{dlog}(X_2 - Y_1 - Y_2)], \end{aligned} \quad (3.27)$$

where we have rescaled $\mathcal{F}_3 \rightarrow -\mathcal{F}_3$, $\tilde{\mathcal{F}}_3 \rightarrow -\tilde{\mathcal{F}}_3$ and $\mathcal{Q}_3 \rightarrow -\mathcal{Q}_3$ allowed by the homogeneous nature.

Collecting all of the canonical differential equations derived above, we have

$$\begin{aligned} d\mathcal{P} = \varepsilon [& \mathcal{P}(l_1 + l_2) + \mathcal{F}_1(l_3 - l_1) + \tilde{\mathcal{F}}_1(l_4 - l_2) + \mathcal{F}_2(l_5 - l_1) + \tilde{\mathcal{F}}_2(l_6 - l_2) \\ & + \mathcal{F}_3(l_7 - l_1) + \tilde{\mathcal{F}}_3(l_8 - l_2)], \\ d\mathcal{F}_1 = \varepsilon [& \mathcal{F}_1(l_2 + l_3) + \mathcal{Q}_1(l_9 - l_2)], & d\tilde{\mathcal{F}}_1 = \varepsilon [\tilde{\mathcal{F}}_1(l_1 + l_4) + \mathcal{Q}_1(l_9 - l_1)], \\ d\mathcal{F}_2 = \varepsilon [& \mathcal{F}_2(l_2 + l_5) + \mathcal{Q}_2(l_{10} - l_2)], & d\tilde{\mathcal{F}}_2 = \varepsilon [\tilde{\mathcal{F}}_2(l_1 + l_6) + \mathcal{Q}_2(l_{10} - l_1)], \\ d\mathcal{F}_3 = \varepsilon [& \mathcal{F}_3(l_2 + l_7) + \mathcal{Q}_3(l_{11} - l_2)], & d\tilde{\mathcal{F}}_3 = \varepsilon [\tilde{\mathcal{F}}_3(l_1 + l_8) + \mathcal{Q}_3(l_{11} - l_1)], \\ d\mathcal{Q}_1 = 2\varepsilon \mathcal{Q}_1 l_9, & \quad d\mathcal{Q}_2 = 2\varepsilon \mathcal{Q}_2 l_{10}, \quad d\mathcal{Q}_3 = 2\varepsilon \mathcal{Q}_3 l_{11}, \end{aligned} \quad (3.28)$$

and taking the limit $\varepsilon \rightarrow 0$, we can obtain

$$\begin{aligned}
d\mathcal{P} &= \mathcal{F}_1(l_3-l_1) + \tilde{\mathcal{F}}_1(l_4-l_2) + \mathcal{F}_2(l_5-l_1) + \tilde{\mathcal{F}}_2(l_6-l_2) + \mathcal{F}_3(l_7-l_1) + \tilde{\mathcal{F}}_3(l_8-l_2), \\
d\mathcal{F}_1 &= \mathcal{Q}_1(l_9-l_2), \quad d\tilde{\mathcal{F}}_1 = \mathcal{Q}_1(l_9-l_1), \quad d\mathcal{F}_2 = \mathcal{Q}_2(l_{10}-l_2), \quad d\tilde{\mathcal{F}}_2 = \mathcal{Q}_2(l_{10}-l_1), \\
d\mathcal{F}_3 &= \mathcal{Q}_3(l_{11}-l_2), \quad d\tilde{\mathcal{F}}_3 = \mathcal{Q}_3(l_{11}-l_1), \quad d\mathcal{Q}_1 = d\mathcal{Q}_2 = d\mathcal{Q}_3 = 0,
\end{aligned} \tag{3.33}$$

where it is not difficult to check the matrix \tilde{A}_{dS} obeys the integrability conditions (3.14). Subsequently, based on the differential equations (3.33), we can derive the symbol for two-site one-loop correlator:

$$\begin{aligned}
\mathcal{S}_2^{(1)} &= (w_9/w_2) \otimes (w_3/w_1) + (w_9/w_1) \otimes (w_4/w_2) \\
&\quad + (w_{10}/w_2) \otimes (w_5/w_1) + (w_{10}/w_1) \otimes (w_6/w_2) \\
&\quad + (w_{11}/w_2) \otimes (w_1/w_7) + (w_{11}/w_1) \otimes (w_2/w_8),
\end{aligned} \tag{3.34}$$

where we revert the previously rescaled \mathcal{F}_3 and \mathcal{Q}_3 back to their original forms. Further, by using the *PolyLogTools* package [20], we can derive the transcendental function with transcendental degree-2 after integrating the symbol (3.34),

$$\begin{aligned}
f_2^{(1)} &= -\pi^2/6 + \text{Li}_2(w_3/w_9) + \text{Li}_2(w_4/w_9) + \text{Li}_1(w_3/w_9)\text{Li}_1(w_4/w_9) \\
&\quad + \text{Li}_2(w_5/w_{10}) + \text{Li}_2(w_6/w_{10}) + \text{Li}_1(w_5/w_{10})\text{Li}_1(w_6/w_{10}) \\
&\quad - \text{Li}_2(w_7/w_{11}) - \text{Li}_2(w_8/w_{11}) - \text{Li}_1(w_7/w_{11})\text{Li}_1(w_8/w_{11}).
\end{aligned} \tag{3.35}$$

Both $\mathcal{S}_2^{(1)}$ and $f_2^{(1)}$ are consistent with the results presented in Ref. [21]. This alignment reinforces the correctness of our method and demonstrates that our approach accurately captures the underlying physical relationships, contributing to a reliable interpretation of the two-site one-loop graph in de Sitter space.

3.2 Two-Site One-Loop Tadpole

At two-site one-loop, another topology is the tadpole contribution which is shown in Fig. 3. The wavefunction coefficient for a tadpole graph, when approached from the perspective of positive geometry [17], corresponds to a cosmological polytope with the structure of a square pyramid [3]. This square pyramid polytope can be effectively triangulated and divided into two distinct zero-edge-weight smaller polytopes. Notably, the pole structures of these smaller polytopes mirror those found in tree-level diagrams, which enables us to impose techniques from Refs. [7, 8] to compute the corresponding differential equations for

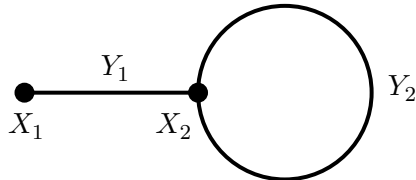


Figure 3. The Feynman diagram for the two-site one-loop tadpole wavefunction coefficient.

analyzing the differential system. Further detailed elaboration on this computation method is not included here.

We start by computing the wavefunction coefficient for two-site one-loop tadpole graph in flat spacetime:

$$\begin{aligned}\psi_{2,\text{Mink}}^{(1)\text{tad}} &= i^2 \int_{-\infty}^0 d\eta_1 \int_{-\infty}^0 d\eta_2 K(X_1; \eta_1) K(X_2; \eta_2) G(Y_1; \eta_1, \eta_2) G(Y_2; \eta_2, \eta_2) \\ &= \frac{X_1 + Y_1 + 2(X_2 + Y_2)}{(X_1 + X_2)(X_1 + Y_1)(X_2 + Y_1)(X_1 + X_2 + 2Y_2)(X_2 + Y_1 + 2Y_2)}.\end{aligned}\quad (3.36)$$

The FRW wavefunction coefficient for tadpole can be obtained by imposing the energy shifts: $(X_1, X_2) \rightarrow (X_1 + x_1, X_2 + x_2)$ on its flat-space form. After incorporating the twister and normalization factors, we have

$$\begin{aligned}\psi_{2,\text{FRW}}^{(1)\text{tad}} &= 4Y_1 Y_2 \int dx_1 \wedge dx_2 (x_1 x_2)^\varepsilon \psi_{2,\text{Mink}}^{(1)\text{tad}} \Big|_{\substack{X_1 \rightarrow X_1 + x_1 \\ X_2 \rightarrow X_2 + x_2}} \\ &= -2Y_1 \int dx_1 \wedge dx_2 (T_1 T_2)^\varepsilon \left(\frac{1}{L_1 \bar{L}_2 D_2} - \frac{1}{L_1 L_2 D_3} \right) \equiv \int d\mu \bar{\Omega}_{\mathcal{P}}^2,\end{aligned}\quad (3.37)$$

where the hyperplanes are defined as follows:

$$\begin{aligned}T_1 &= x_1, & T_2 &= x_2, \\ L_1 &= x_1 + X_1 + Y_1, & L_2 &= x_2 + X_2 + Y_1, & \bar{L}_2 &= L_2 + 2Y_2, \\ D_2 &= x_1 + x_2 + X_1 + X_2 + 2Y_2, & D_3 &= x_1 + x_2 + X_1 + X_2.\end{aligned}\quad (3.38)$$

Similar to the analysis of bubble diagram, in Eq. (3.38), those hyperplanes can be arranged in (x_1, x_2) -plane as illustrated in Fig. 4. In this factorization, one term is exactly tree function and the other is a shifted tree with $X_2 \rightarrow X_2 + 2Y_2$. This observation enable us to immediately read out the differential equations obeyed by the tadpole system, which is nothing but a linear combination of the two tree-level systems. Therefore, the total integral family contains eight independent members which can be divided into two sets:

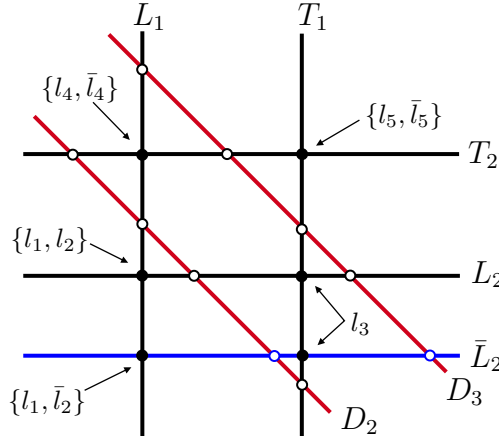


Figure 4. The hyperplane arrangement for the two-site one-loop tadpole wavefunction coefficient.

$\mathbf{F}_2 = \{\mathcal{P}_2, \mathcal{F}_2, \tilde{\mathcal{F}}_2, \mathcal{Q}_2\}$ and $\mathbf{F}_3 = \{\mathcal{P}_3, \mathcal{F}_3, \tilde{\mathcal{F}}_3, \mathcal{Q}_3\}$. The associated canonical forms for $\mathbf{F}_2, \mathbf{F}_3$ are defined in the similar way of Eq. (3.7):

$$\text{Layer-0: } \bar{\Omega}_{\mathcal{P}_2}^2 = \frac{-2Y_1}{L_1 \bar{L}_2 D_2}, \quad \bar{\Omega}_{\mathcal{P}_3}^2 = \frac{-2Y_1}{L_1 L_2 D_3}, \quad (3.39a)$$

$$\text{Layer-1: } \bar{\Omega}_{\mathcal{F}_2}^2 = \frac{X_1 - Y_1}{T_1 \bar{L}_2 D_2}, \quad \bar{\Omega}_{\mathcal{F}_3}^2 = \frac{X_1 - Y_1}{T_1 L_2 D_3}, \quad (3.39b)$$

$$\bar{\Omega}_{\tilde{\mathcal{F}}_2}^2 = \frac{X_2 - Y_1 + 2Y_2}{T_2 L_1 D_2}, \quad \bar{\Omega}_{\tilde{\mathcal{F}}_3}^2 = \frac{X_2 - Y_1}{T_2 L_1 D_3} \quad (3.39c)$$

$$\text{Layer-2: } \bar{\Omega}_{\mathcal{Q}_2}^2 = \frac{X_1 + X_2 + 2Y_2}{T_1 T_2 D_2}, \quad \bar{\Omega}_{\mathcal{Q}_3}^2 = \frac{X_1 + X_2}{T_1 T_2 D_3}. \quad (3.39d)$$

Notably, unlike in the bubble case, the D_1 plane in the hyperplane arrangement (cf. Fig. 3) transforms into the plane \bar{L}_2 which is parallel to T_2 and L_2 in the tadpole configuration (cf. Fig. 4). This transformation eliminates the presence of \mathbf{F}_1 in the bubble case. Meanwhile, the definitions of canonical forms for \mathbf{F}_2 and \mathbf{F}_3 in Eq. (3.39) remain similar to those in bubble case (3.7), albeit with some slight modifications to the definition of hyperplanes.

Then, the canonical DEs associated with Eq. (3.39) can be derived as follows:

$$\begin{aligned} d\mathcal{P}_2 &= \varepsilon [\mathcal{P}_2(l_1 + \bar{l}_2) + \mathcal{F}_2(l_3 - l_1) + \tilde{\mathcal{F}}_2(\bar{l}_4 - \bar{l}_2)], \\ d\mathcal{P}_3 &= \varepsilon [\mathcal{P}_3(l_1 + l_2) + \mathcal{F}_3(l_3 - l_1) + \tilde{\mathcal{F}}_3(l_4 - l_2)], \\ d\mathcal{F}_2 &= \varepsilon [\mathcal{F}_2(\bar{l}_2 + l_3) + \mathcal{Q}_2(\bar{l}_5 - \bar{l}_2)], \quad d\tilde{\mathcal{F}}_2 = \varepsilon [\tilde{\mathcal{F}}_2(l_1 + \bar{l}_4) + \mathcal{Q}_2(\bar{l}_5 - l_1)], \\ d\mathcal{F}_3 &= \varepsilon [\mathcal{F}_3(l_2 + l_3) + \mathcal{Q}_3(l_5 - l_2)], \quad d\tilde{\mathcal{F}}_3 = \varepsilon [\tilde{\mathcal{F}}_3(l_1 + l_4) + \mathcal{Q}_3(l_5 - l_1)], \\ d\mathcal{Q}_2 &= 2\varepsilon \mathcal{Q}_1 \bar{l}_5, \quad d\mathcal{Q}_3 = 2\varepsilon \mathcal{Q}_2 l_5, \end{aligned} \quad (3.40)$$

where the letters are given by

$$\begin{aligned} l_1 &= \text{dlog}(X_1 + Y_1), & l_2 &= \text{dlog}(X_2 + Y_1), & \bar{l}_2 &= \text{dlog}(X_2 + Y_1 + 2Y_2), \\ l_3 &= \text{dlog}(X_1 - Y_1), & l_4 &= \text{dlog}(X_2 - Y_1), & \bar{l}_4 &= \text{dlog}(X_2 - Y_1 + 2Y_2), \\ l_5 &= \text{dlog}(X_1 + X_2), & \bar{l}_5 &= \text{dlog}(X_1 + X_2 + 2Y_2). \end{aligned} \quad (3.41)$$

Taking the dS limit $\varepsilon \rightarrow 0$, Eq. (3.40) will reduce to the following forms:

$$\begin{aligned} d\mathcal{P}_2 &= \mathcal{F}_2(l_3 - l_1) + \tilde{\mathcal{F}}_2(\bar{l}_4 - \bar{l}_2), & d\mathcal{P}_3 &= \mathcal{F}_3(l_3 - l_1) + \tilde{\mathcal{F}}_3(l_4 - l_2) \\ d\mathcal{F}_2 &= \mathcal{Q}_2(\bar{l}_5 - \bar{l}_2), & d\tilde{\mathcal{F}}_2 &= \mathcal{Q}_2(\bar{l}_5 - l_1), \\ d\mathcal{F}_3 &= \mathcal{Q}_3(l_5 - l_2), & d\tilde{\mathcal{F}}_3 &= \mathcal{Q}_3(l_5 - l_1), \\ d\mathcal{Q}_2 &= d\mathcal{Q}_3 = 0, \end{aligned} \quad (3.42)$$

where one can write the symbol results:

$$\begin{aligned} \mathcal{S}_2^{(1)} &= (\bar{w}_5/\bar{w}_2) \otimes (w_3/w_1) + (\bar{w}_5/w_1) \otimes (\bar{w}_4/\bar{w}_2) \\ &\quad + (w_5/w_2) \otimes (w_3/w_1) + (w_5/w_1) \otimes (w_4/w_2), \end{aligned} \quad (3.43)$$

and the transcendental function after integrating the symbol (3.43)

$$f_2^{(1)} = -\pi^2/6 + \text{Li}_2(w_3/w_5) + \text{Li}_2(w_4/w_5) + \text{Li}_1(w_3/w_5)\text{Li}_1(w_4/w_5) \\ + \text{Li}_2(w_3/\bar{w}_5) + \text{Li}_2(\bar{w}_4/\bar{w}_5) + \text{Li}_1(\bar{w}_3/\bar{w}_5)\text{Li}_1(\bar{w}_4/\bar{w}_5), \quad (3.44)$$

where $l_i = \text{dlog}(w_i)$ and $\bar{l}_i = \text{dlog}(\bar{w}_i)$.

Further, a closer look at the tadpole differential system (3.40) reveals distinct features against the bubble system. Importantly, the two parent functions \mathcal{P}_2 and \mathcal{P}_3 cannot be merged into a single one \mathcal{P} like the bubble case without spoiling the uniform transcendental property. This distinction arises because the calculation of the DEs for \mathcal{P}_2 and \mathcal{P}_3 involves matching the residues at two different codimension-2 boundaries: the intersections $L_1 \cap L_2$ and $L_1 \cap \bar{L}_2$. Each of these intersections generates a distinct dlog singularities i.e., l_2 and \bar{l}_2 , preventing the two parent functions from being merged into single one. In contrast, for the bubble case, all parent functions share a single codimension-2 boundary, $L_1 \cap L_2$.

Another intriguing feature is that the tadpole wavefunction coefficient, unlike the bubble case, does not “see” the entire system. Specifically, only eight basis functions contribute to the tadpole canonical differential equations, despite the configuration of hyperplane arrangement indicating a 10-dimensional vector space. This selective probing of a subset of the full cohomology space is expected to be a recurring phenomenon as the diagram’s complexity increases. For instance, even at tree level, the three-site diagram explores only a 16-dimensional subspace within the full 25-dimensional space given by cohomology [8]. This observation highlights that the physical observables possess unique properties not shared by generic mathematical constructs.

For the two-site case, we have the advantage of explicitly identifying the part unseen by the tadpole function. The hyperplane arrangement indicates a total of twelve canonical forms, representing all possible triangles bounded by seven planes (3.38), with $12 = 3 \times 2 \times 2$. In addition to the eight 2-forms given in Eq. (3.39), the remaining four 2-forms, defined with the previously established positive orientation, are given by:

$$\bar{\Omega}_{\mathcal{O}_2}^2 = \frac{-2(Y_1 - Y_2)}{L_1 L_2 D_2}, \quad \bar{\Omega}_{\mathcal{O}_3}^2 = \frac{-2(Y_1 + Y_2)}{L_1 \bar{L}_2 D_3}, \quad (3.45a)$$

$$\bar{\Omega}_{\mathcal{R}_2}^2 = \frac{X_1 - Y_1 + 2Y_2}{T_1 L_2 D_2}, \quad \bar{\Omega}_{\mathcal{R}_3}^2 = \frac{X_1 - Y_1 - 2Y_2}{T_1 \bar{L}_2 D_3}. \quad (3.45b)$$

As in the bubble case, the twelve 2-forms (3.7) are actually over complete and subjected to two linear constraints induced by the corresponding triangulation relations (3.9), which reduce the number of the independent basis down to ten. While in the tadpole case, since the two disjoint tree systems have already provided eight independent basis, we will need two relations involving the above four extra 2-forms. Explicitly, the triangulation gives the following nontrivial relations:

$$\bar{\Omega}_{\mathcal{P}_3}^2 + \bar{\Omega}_{\mathcal{P}_2}^2 - \bar{\Omega}_{\mathcal{O}_3}^2 - \bar{\Omega}_{\mathcal{O}_2}^2 + \bar{\Omega}_{\mathcal{R}_3}^2 + \bar{\Omega}_{\mathcal{R}_2}^2 - \bar{\Omega}_{\mathcal{F}_3}^2 - \bar{\Omega}_{\mathcal{F}_2}^2 = 0, \quad (3.46a)$$

$$\bar{\Omega}_{\mathcal{P}_3}^2 - \bar{\Omega}_{\mathcal{O}_2}^2 - \bar{\Omega}_{\mathcal{F}_3}^2 - \bar{\Omega}_{\tilde{\mathcal{F}}_3}^2 + \bar{\Omega}_{\tilde{\mathcal{F}}_2}^2 + \bar{\Omega}_{\mathcal{R}_2}^2 + \bar{\Omega}_{\mathcal{Q}_3}^2 - \bar{\Omega}_{\mathcal{Q}_2}^2 = 0. \quad (3.46b)$$

In principle, we have freedom to choose two of these four as our basis. For example, if we choose \mathcal{O}_2 , the total derivative would be sketched as:

$$d\mathcal{O}_2 \sim \mathcal{O}_2 + \mathcal{R}_2 + \tilde{\mathcal{F}}_2, \quad (3.47)$$

where \mathcal{R}_2 should be re-expressed in terms of basis functions. Then, from Eq. (3.46) the spanning basis should further include either \mathcal{R}_3 or \mathcal{O}_3 . For example, the IBP for \mathcal{R}_3 is derived in Appendix A.1 and the corresponding canonical DE is

$$d\mathcal{R}_3 = \varepsilon \left[\mathcal{R}_3 d\log(X_1 - Y_1 - 2Y_2) + (\mathcal{R}_3 - \mathcal{Q}_3) d\log(X_2 + Y_1 + 2Y_2) + \mathcal{Q}_3 d\log(X_1 + X_2) \right]. \quad (3.48)$$

Although the whole system is now solved, we see that in this basis the differentiation of \mathcal{O}_2 interacts with \mathcal{R}_2 , which in turn couples to the \mathcal{P} , \mathcal{F} , and \mathcal{Q} . This means the DE of \mathcal{O}_2 is not UT but instead mixes with basis across all layers and tree systems. However, a more efficient basis choice involves including $\{\mathcal{R}_2, \mathcal{R}_3\}$. The IBP of \mathcal{R}_2 is worked out in the appendix and the DE reads

$$d\mathcal{R}_2 = \varepsilon \left[\mathcal{R}_2 d\log(X_1 - Y_1 + 2Y_2) + (\mathcal{R}_2 - \mathcal{Q}_2) d\log(X_2 + Y_1) + \mathcal{Q}_2 d\log(X_1 + X_2 + 2Y_2) \right]. \quad (3.49)$$

Together, the basis $\{\mathcal{P}_3, \mathcal{F}_3, \tilde{\mathcal{F}}_3, \mathcal{R}_3, \mathcal{Q}_3, \mathcal{P}_2, \mathcal{F}_2, \tilde{\mathcal{F}}_2, \mathcal{R}_2, \mathcal{Q}_2\}$ defines the *whole system* DEs. The benefit for this choice of the basis is that each DE is UT and the mixing is minimized, especially with the two additional basis falling separately into the two disjoint tree systems without mixing them up.

The study of complete hyperplane arrangement suggests a *tailored basis* for both the tadpole wavefunction and the whole system. The DE structure of $\{\mathcal{R}_2, \mathcal{R}_3\}$ being simpler than that of $\{\mathcal{O}_2, \mathcal{O}_3\}$ is expected from IBP. After trading the differentiation of external energy for that of the twister variables, the IBP of $\partial_{x_{1,2}}$ will only generate $T_{1,2}$ -poles correspondingly. Since $\mathcal{R}_{2,3}$ already have one T pole, after IBP they can only talk to themselves and Q functions through residue matching, while with two L -poles $\mathcal{O}_{2,3}$ have chance to talk to all of the \mathcal{R} and \mathcal{F} functions. This suggests us to first choose the canonical forms with more T -poles as basis when we have freedom to do so.

Comparing with closed projective simplex basis Our approach of IBP on triangle canonical forms is a special case of the systematic procedure in Ref. [8] using boundary-less linear combination of projective simplex forms. Namely, in integration space \mathbb{R}^p , define projective simplex p -forms involving all possible p -tuples of planes as:

$$[L_1 \cdots L_p] \equiv d\log L_1 \wedge \cdots \wedge d\log L_p, \quad (3.50)$$

together with the boundary operator

$$\partial[L_1 \cdots L_p] \equiv \sum_{r=1}^p (-1)^{r+1} [L_1 \cdots \hat{L}_r \cdots L_p], \quad (3.51)$$

where boundaryless means closed under ∂ . These projective p -forms are the canonical forms of the simplex formed from the intersection of the p hyperplanes with the plane at infinity L_∞ . It is straightforward to verify that the boundary operator satisfies $\partial^2 = 0$, and the linear combination of projective p -forms are closed under ∂ correspond to bounded regions in \mathbb{R}^p , forming the basis of the twisted integral. Specifically, any p -simplex (not projective simplex) in \mathbb{R}^p defined by $p + 1$ hyperplanes, is exact and hence closed:

$$\Omega_{p\text{-simplex}} = \partial[L_1 \cdots L_{p+1}], \quad (3.52)$$

with simplest examples being triangle canonical forms defined by $\Omega_\Delta = \text{dlog}(\frac{L_i}{L_k}) \wedge \text{dlog}(\frac{L_j}{L_k})$. The iterative emerging of T -poles under IBP corresponds to a formula holds inside of a twisted integral, which is proved in Ref. [8]:

$$\text{d}[L_1 \cdots L_n] = \varepsilon \sum_a \text{dlog} \langle \hat{T}_a \hat{L}_1 \cdots \hat{L}_p \rangle \times \partial[T_a L_1 \cdots L_p], \quad (3.53)$$

where

$$L_a \equiv \hat{L}_a \cdot P, \quad P^I \equiv (1, x_1, \cdots, x_p), \quad \langle \hat{L}_1 \cdots \hat{L}_{p+1} \rangle \equiv \det(\hat{L}_1, \cdots, \hat{L}_{p+1}). \quad (3.54)$$

The general strategy involves expressing the wavefunction as a closed linear combination of Eq. (3.50), applying Eq. (3.53), and iteratively adding new functions to the basis as new letters appear. However, diverging from this comprehensive approach, we find it more practical in many cases to use bounded simplex regions as the basis. This choice minimizes mixing between different basis elements during differentiation. Explicitly, we employ a bottom-up strategy: we exhaust a priori the independent closed linear combinations of Eq. (3.50) with more twist T -planes and ensure that each form aligns with the simplex representation in Eq. (3.52).

The tailored basis for tadpole system suggests a *preferred triangle basis* suitable for 2-dimensional two-site systems with general loop number and topology. We denote $\{\mathcal{P}, \mathcal{F}, \mathcal{Q}\}$ as top, middle, and bottom layer functions and state our procedure to exhaust preferred triangle basis:

- First, exhaust \mathcal{Q} -basis with two T -poles as $\partial[T_1 T_2 D_k]$, with D_k running for all “diagonal” lines. Since IBP will only generate extra $T_{1,2}$ -poles, they will only talk to themselves, serving as bottom-layer functions.
- Next, exhaust mid-layer \mathcal{F} -basis with one T -pole and one L -pole as $\partial[T_i L_j D_k]$, which amounts to replacing one T -pole with parallel L -poles in \mathcal{Q} -basis. Any new T -pole generated by IBP will be parallel to L_j , so that the only closed objects sharing the common pole structure are itself and the bottom-layer ones already exhausted.
- Top-layer functions suggest themselves as solely L -poles after we exhaust all the T -pole basis, which look like $\partial[L_i L_j D_k]$. How many different L -pairs appear in the remaining basis shows the number of top-layer functions. After IBP they will in general talk to themselves and the corresponding two L -branches of \mathcal{F} function. They serve as parent functions for the whole differential system.

\mathcal{P}_i would mix these blocks. This behavior is intuitive from a geometric perspective: among all linearly bounded regions, simplices exhibit the minimal number of codimension-1 poles in their canonical forms.

3.3 New Features of Hyperplane Arrangement at Loop Level

Our detailed investigation of loop-level hyperplane arrangements and their associated differential systems reveals several distinct features absent at tree level, summarized as follows:

- **Ambiguity in Parent Function Definition:** At loop level, defining the parent function based solely on the hyperplane arrangement is ambiguous, and the differential system may involve multiple parent functions. Unlike tree-level systems, where a unique, boundary-less object directly corresponds to the cosmological wavefunction of interest and does not involve twisted planes, this uniqueness does not hold for loop-level cases such as the bubble or tadpole systems. For example, the tadpole system necessarily requires two parent functions to span the system. This ambiguity arises from the parallel L - and D -lines in hyperplane arrangements generated by loop diagrams, which contrasts with tree systems where all lines intersect. And this distinction is particularly evident in the tubing approach to wavefunction coefficients; see tree examples in Ref. [8] and loop-level cases in Eq. (4.1) and Eq. (4.18).
- **Reduced Basis Size for Canonical DEs:** At loop level, the number of basis functions relevant to the canonical differential equations is typically smaller than that at tree level with the same number of internal edges. For tree-level systems, the number of basis functions scales as 4^e where e being the number of the internal edges. In contrast, our analysis shows that the one-loop bubble has 10 basis functions, the tadpole has 8, and the two-site two-loop sunrise has 22, two-site arbitrary loop has $3 \cdot 2^e - 2$ [cf. Eq. (B.6)]. The slower scaling of the relevant vector space dimension at loop level is expected, as the numerous parallel lines appearing in loop hyperplane arrangements make the hyperplane arrangements highly nontrivial, and indicate that the wavefunction of physical interest have special features that distinguish them from generic mathematical objects.

4 Kinematic Flow for Two-Site One-Loop Graph

In this section, we apply the tubing graph framework to study the differentiation system for two-site one-loop correlators. For the first time, we extend the tree-level tubing framework [7, 8] to the loop-level. We introduce the graphical rules governing loop-level tubings and present a systematic methodology for deriving the associated canonical differential equations. This approach significantly simplifies the derivation process, reducing it to a set of universal and widely applicable principles.

4.1 Two-Site One-Loop Bubble

As illustrated in Ref. [1], the wavefunction coefficient for a given graph can be obtained by summing over all possible ways of iteratively dividing the graph into connected tubes³, each tube graph associated with the inverse of the sum of its total energies. For two-site one-loop bubble graph, there are two ways to divide the graph into two subgraphs:

$$\psi_{2,(a)}^{(1)\text{bub}} = \text{Diagram} = \frac{1}{X_1+Y_1+Y_2} \times \frac{1}{X_2+Y_1+Y_2} \times \frac{1}{X_1+X_2+2Y_1} \times \frac{1}{X_1+X_2}, \quad (4.1a)$$

$$\psi_{2,(b)}^{(1)\text{bub}} = \text{Diagram} = \frac{1}{X_1+Y_1+Y_2} \times \frac{1}{X_2+Y_1+Y_2} \times \frac{1}{X_1+X_2+2Y_2} \times \frac{1}{X_1+X_2}, \quad (4.1b)$$

where each subgraph contains four tubes. Summing over the two contributions in Eq. (4.1), we can obtain the full wavefunction coefficient $\psi_{2,\text{Mink}}^{(1)\text{bub}}$ as computed in Eq. (3.1).

Given that tubes can reflect the singularities, we aim to establish a connection between tubings and the canonical DEs. To achieve it, we use the property that kinematic data can flow along the internal lines, driving the evolution of the tubes. And we will adopt a similar approach as established at the tree level [8], where the cross sign “ \times ” are dressed on the internal lines. These marks indicate that the kinematic variables flow along these intermediate edges. Then, the letters appearing in DEs are then depicted as the connected tubes, which are formed by encircling the vertices or both of the vertices and the cross signs in a graph. These are characterized as follows:

- If a tube graph encircles only a single vertex, it corresponds to a dlog form of the sum of the energy associated with that vertex and the all of the energies associated with the internal lines intersected by the tube.
- If the tube graph encircles both a vertex and its adjacent internal lines marked with cross signs, the corresponding dlog form requires flipping the sign of the energies associated with those marked internal lines.
- If the tube graph contains more than one vertex, then the energies associated with the marked internal lines between any two enclosed vertices will vanish in its associated dlog expression.

Therefore, all of the letters (3.29) can be represented as marked tubing graphs which are summarized in table 1.

The functions within the integral family (3.11) can be represented as a set of complete tubes [7, 8]. In this representation, the tube graphs corresponding to the parent function exclude cross signs, while those for descendant functions include at least one cross sign.

³Different conventions exist regarding whether the outermost tube, which contains all vertices, should be included. Such as Refs. [14–16] choose to omit it, whereas in our work, we consistently include it.

l_1		$\text{dlog}(X_1+Y_1+Y_2)$	l_2		$\text{dlog}(X_2+Y_1+Y_2)$
l_3		$\text{dlog}(X_1+Y_1-Y_2)$	l_4		$\text{dlog}(X_2+Y_1-Y_2)$
l_5		$\text{dlog}(X_1-Y_1+Y_2)$	l_6		$\text{dlog}(X_2-Y_1+Y_2)$
l_7		$\text{dlog}(X_1-Y_1-Y_2)$	l_8		$\text{dlog}(X_2-Y_1-Y_2)$
l_9		$\text{dlog}(X_1+X_2+2Y_1)$	l_{10}		$\text{dlog}(X_1+X_2+2Y_2)$
l_{11}		$\text{dlog}(X_1+X_2)$			

Table 1. The alphabet for the two-site one-loop bubble-type wavefunction coefficient, where the letters $l_i = \text{dlog}(w_i)$.

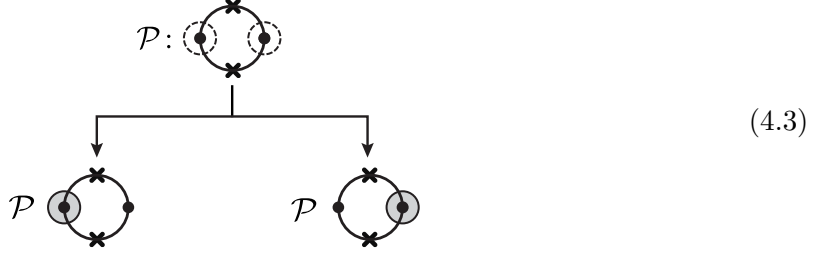
These functions can be systematically categorized into three distinct layers as presented in Eq. (3.6), their explicit forms can be expressed as follows:

Layer-0		
Layer-1	\mathcal{F}_1 $\tilde{\mathcal{F}}_1$ \mathcal{F}_2 $\tilde{\mathcal{F}}_2$ \mathcal{F}_3 $\tilde{\mathcal{F}}_3$ (4.2)	
Layer-2	\mathcal{Q}_1 \mathcal{Q}_2 \mathcal{Q}_3	

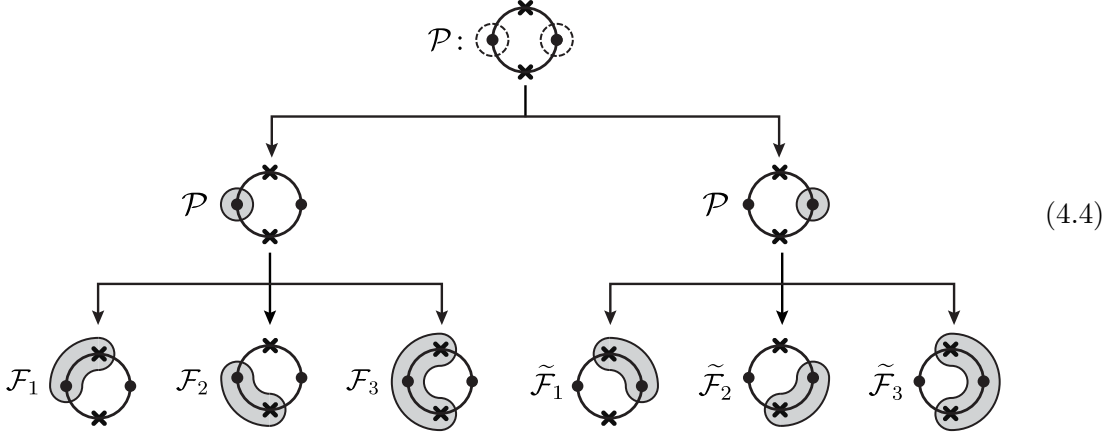
where they are categorized into three layers according to Eq. (3.6). In addition, in Eq. (4.2), dashed lines are used to depict tube graphs, serving as “seeds” that form the foundational building blocks for constructing more intricate structures. Activating these seed tubes sequentially will generate new branches, collectively forming a family tree. Each activated tube is corresponding to a specific letter, enabling a systematic derivation of the DEs governing the system.

Now, we focus on the graph of the parent function \mathcal{P} to show how it works. We will construct the family tree for \mathcal{P} step by step. Firstly, activating the tubes of \mathcal{P} generates

two branches, each one is corresponding to a distinct letter,



where for each branch in the tree, we have also assigned the function associated with the tube graph. Next, each activated tube in Eq. (4.3) that does not contain a cross sign can “grow” to enclose all of its adjacent cross signs in all possible ways. Each distinct growth pathway generates new branches of the family tree:



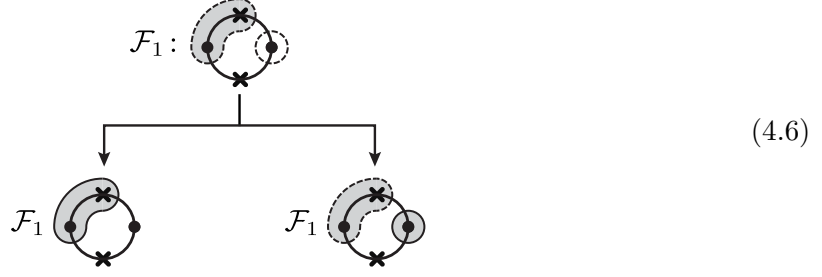
where we have assigned the descendant functions $\{\mathcal{F}_i\}$ and $\{\tilde{\mathcal{F}}_i\}$ associated with the tubes in the third layer of Eq. (4.4). Finally, to obtain the differential equation for parent function \mathcal{P} from the family tree (4.4), we multiply each tube (letter) by the difference between its corresponding function and the sum of the functions associated with all its descendant tube graphs, scaled by a constant factor ε :

$$\begin{aligned}
 d\mathcal{P} &= \varepsilon \left[\left(\mathcal{P} - \sum_{i=1}^3 \mathcal{F}_i \right) l_1 + \left(\mathcal{P} - \sum_{i=1}^3 \tilde{\mathcal{F}}_i \right) l_2 + \sum_{i=1}^3 \mathcal{F}_i l_{2i+1} + \sum_{i=1}^3 \tilde{\mathcal{F}}_i l_{2i+2} \right] \\
 &= \varepsilon \left[\mathcal{P}(l_1 + l_2) + \mathcal{F}_1(l_3 - l_1) + \tilde{\mathcal{F}}_1(l_4 - l_2) + \mathcal{F}_2(l_5 - l_1) + \tilde{\mathcal{F}}_2(l_6 - l_2) \right. \\
 &\quad \left. + \mathcal{F}_3(l_7 - l_1) + \tilde{\mathcal{F}}_3(l_8 - l_2) \right], \tag{4.5}
 \end{aligned}$$

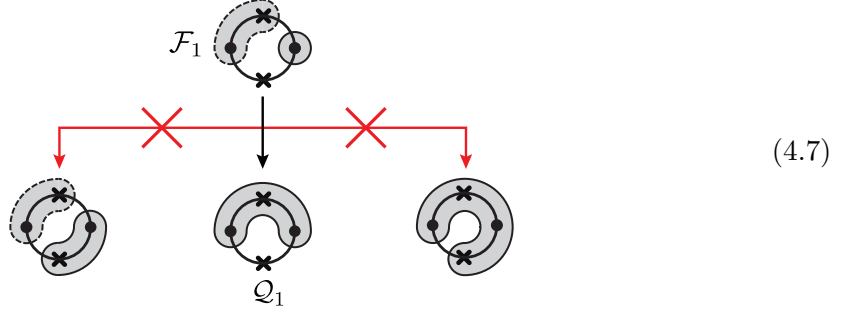
where the letters $\{l_i\}$ are summarized in table 1. As we proceed with the activation and growth process, we can see each newly activated tube generates additional branches, expanding the family tree and manifesting the structure underlying the differential equations through the graphical representation.

Next, we move to study the descendant functions \mathcal{F}_1 and $\tilde{\mathcal{F}}_1$ in layer-1. For the function \mathcal{F}_1 , the two dashed tubes in the graph of \mathcal{F}_1 can be activated independently, forming two

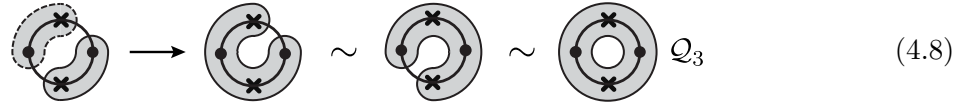
different branches:



where in the second branch of Eq. (4.6), the activated tube can continue to grow and enclose its adjacent cross signs in three different ways:



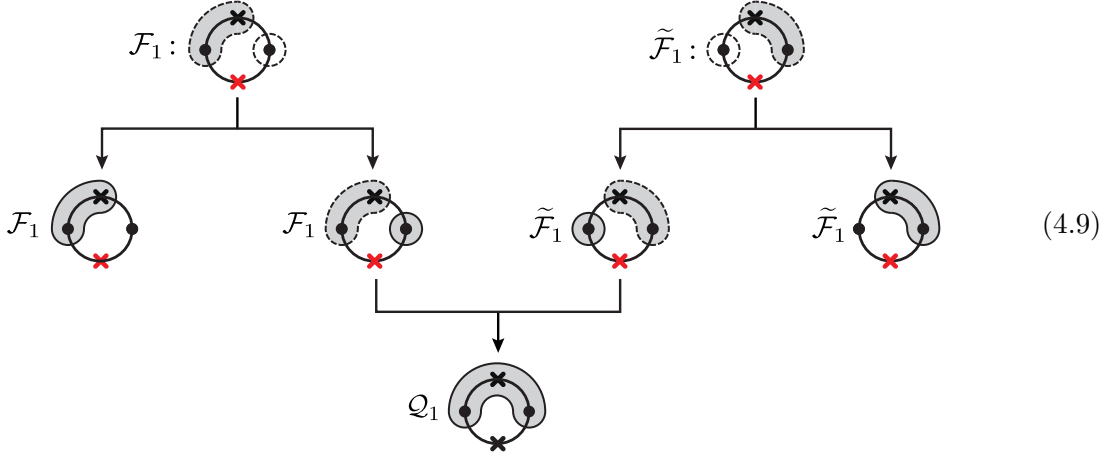
Notice that in Eq. (4.7), we have used red arrows to mark the first and third branches, indicating that the activated tube cannot evolve further into these two branches. In the first branch of Eq. (4.7), the newly formed tube will “merge” with its neighboring tube to create a larger tube. In the third branch of Eq. (4.7), the activated tube directly encloses the cross signs above and below it. As a result, the tube graphs evolve in the first and third branch are topologically equivalent:



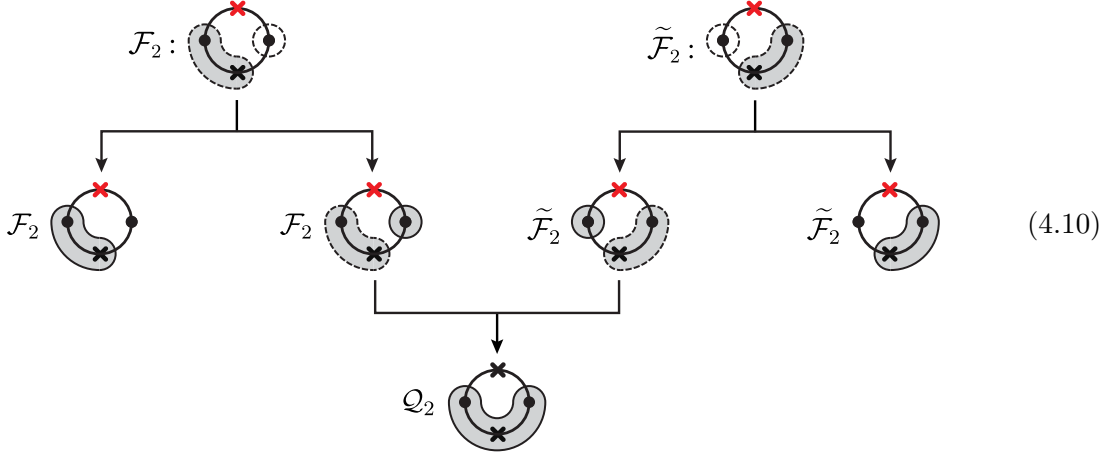
where the final descendant tube of (4.8) is associated with the function Q_3 which should correspond to the ultimate tube graph in the family tree of \mathcal{F}_3 and $\tilde{\mathcal{F}}_3$ (we will discuss it later). Further, the subsystem of hyperplane arrangement for \mathcal{F}_1 is solely related to the planes $\{T_1, T_2, L_1, L_2, D_1\}$. However, the final tube in Eq. (4.8) is related to the planes $\{T_1, T_2, D_3\}$, and D_3 clearly should not appear in the hyperplane system associated with \mathcal{F}_1 . Therefore, \mathcal{F}_1 can only evolve along the second branch in Eq. (4.8).

For the function $\tilde{\mathcal{F}}_1$, we can construct its associated family tree using a method similar to that of \mathcal{F}_1 , so we will ignore the detailed process here. Therefore, the complete family

trees for \mathcal{F}_1 and $\tilde{\mathcal{F}}_1$ are constructed as follows:



where the cross signs marked in red color indicate that these crosses are prevented to be enclosed by the activated tube. Similarly, due to the presence of symmetry, the construction of the family trees for \mathcal{F}_2 and $\tilde{\mathcal{F}}_2$ closely mirrors that of \mathcal{F}_1 and $\tilde{\mathcal{F}}_1$. Therefore, we omit the step-by-step derivation and summarize the results as follows:



Hence, the canonical DEs associated with the descendant functions $\{\mathcal{F}_1, \tilde{\mathcal{F}}_1, \mathcal{F}_2, \tilde{\mathcal{F}}_2\}$ can be easily read from the family trees (4.9)-(4.10):

$$d\mathcal{F}_1 = \varepsilon[(\mathcal{F}_1 - \mathcal{Q}_1)l_2 + \mathcal{F}_1 l_3 + \mathcal{Q}_1 l_9] = \varepsilon[\mathcal{F}_1(l_2 + l_3) + \mathcal{Q}_1(l_9 - l_2)], \quad (4.11a)$$

$$d\tilde{\mathcal{F}}_1 = \varepsilon[(\tilde{\mathcal{F}}_1 - \mathcal{Q}_1)l_1 + \mathcal{F}_1 l_4 + \mathcal{Q}_1 l_9] = \varepsilon[\tilde{\mathcal{F}}_1(l_1 + l_4) + \mathcal{Q}_1(l_9 - l_1)], \quad (4.11b)$$

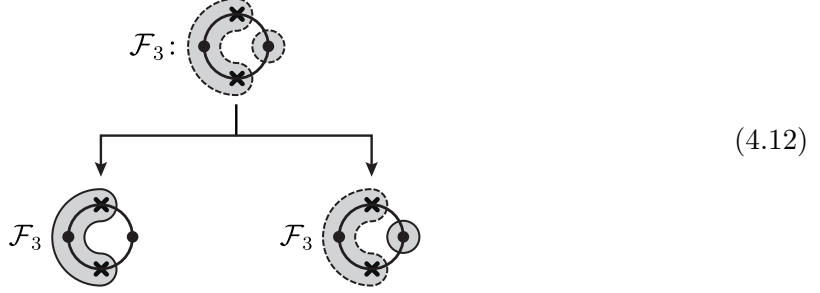
$$d\mathcal{F}_2 = \varepsilon[(\mathcal{F}_2 - \mathcal{Q}_2)l_2 + \mathcal{F}_2 l_5 + \mathcal{Q}_2 l_{10}] = \varepsilon[\mathcal{F}_2(l_2 + l_5) + \mathcal{Q}_2(l_{10} - l_2)], \quad (4.11c)$$

$$d\tilde{\mathcal{F}}_2 = \varepsilon[(\tilde{\mathcal{F}}_2 - \mathcal{Q}_2)l_1 + \tilde{\mathcal{F}}_2 l_6 + \mathcal{Q}_2 l_{10}] = \varepsilon[\tilde{\mathcal{F}}_2(l_1 + l_6) + \mathcal{Q}_2(l_{10} - l_1)], \quad (4.11d)$$

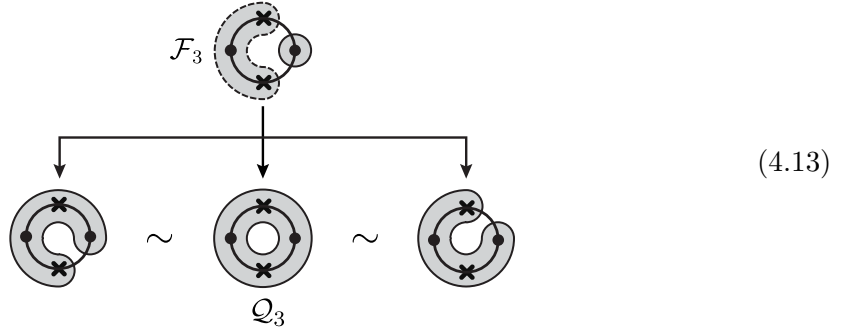
where the letters $\{l_i\}$ are given in table 1. Here, the rules for generating the family trees of $\{\mathcal{F}_1, \tilde{\mathcal{F}}_1, \mathcal{F}_2, \tilde{\mathcal{F}}_2\}$ differ slightly from those at the tree level. This is because, within our chosen basis, the family tree for each subsystem is independent and does not mix with

others. Hence, some graphs that are unique in one family tree do not appear in other family trees.

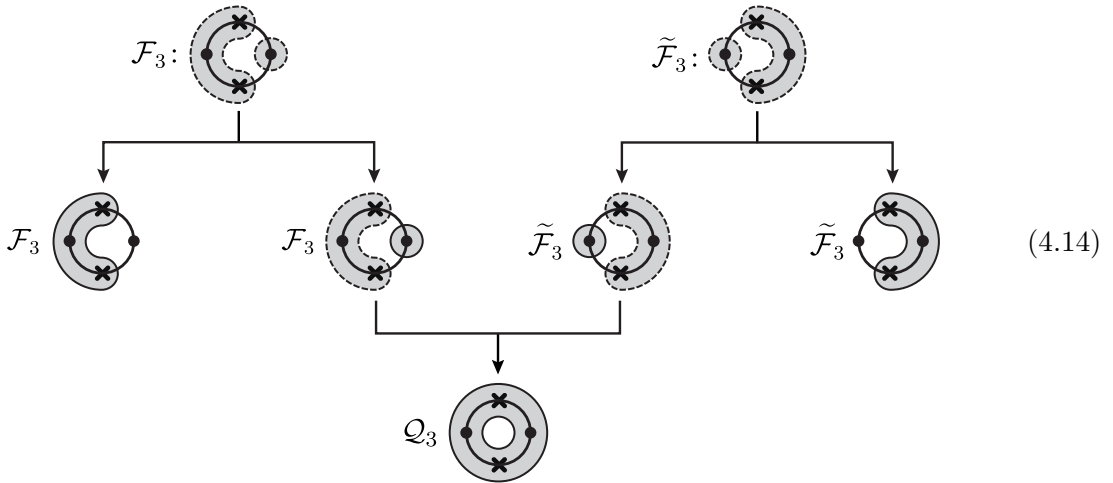
Subsequently, we concentrate on studying the last two descendant functions \mathcal{F}_3 and $\tilde{\mathcal{F}}_3$ in layer-1. Again, for \mathcal{F}_3 , the two dashed tubes in the graph of \mathcal{F}_3 can be activated independently, forming two distinct branches:



In the second branch of Eq. (4.12), the activated tube can continue to grow and encloses the cross sign above, below, or both, thereby forming three branches:



where those three branches are topologically equivalent, reducing the final descendant tube graph to a single configuration, the second branch in Eq. (4.13). A similar approach applies to $\tilde{\mathcal{F}}_3$, yielding a parallel family tree. In summary, the complete family trees associated with \mathcal{F}_3 and $\tilde{\mathcal{F}}_3$ are represented as follows:



Thus, the canonical DEs associated with the functions \mathcal{F}_3 and $\tilde{\mathcal{F}}_3$ can be obtained from the family tree (4.14) as follows:

$$d\mathcal{F}_3 = \varepsilon[(\mathcal{F}_3 - \mathcal{Q}_3)l_2 + \mathcal{F}_3 l_7 + \mathcal{Q}_3 l_{11}] = \varepsilon[\mathcal{F}_3(l_2 + l_7) + \mathcal{Q}_3(l_{11} - l_2)], \quad (4.15a)$$

$$d\tilde{\mathcal{F}}_3 = \varepsilon[(\tilde{\mathcal{F}}_3 - \mathcal{Q}_3)l_1 + \tilde{\mathcal{F}}_3 l_8 + \mathcal{Q}_3 l_{11}] = \varepsilon[\tilde{\mathcal{F}}_3(l_1 + l_8) + \mathcal{Q}_3(l_{11} - l_1)]. \quad (4.15b)$$

Finally, we analyze the three descendant functions $\mathcal{Q}_1, \mathcal{Q}_2$ and \mathcal{Q}_3 in layer-2. In this scenario, the graphs associated with $\{\mathcal{Q}_i\}$ are enclosed by a single tube that becomes activated:

$$(4.16)$$

where the factor of 2 emerges from the enclosure of two vertices within the activated tube. Hence, by referencing the family trees in Eq. (4.16), we can derive the canonical DEs for $\{\mathcal{Q}_i\}$ as follows:

$$d\mathcal{Q}_1 = 2\varepsilon \mathcal{Q}_1 l_9, \quad d\mathcal{Q}_2 = 2\varepsilon \mathcal{Q}_2 l_{10}, \quad d\mathcal{Q}_3 = 2\varepsilon \mathcal{Q}_3 l_{11}. \quad (4.17)$$

Collecting Eqs. (4.11), (4.15) and (4.16), we can check that they are consistent with the results (3.28) derived by using the methods of hyperplane arrangement and IBP.

4.2 Two-Site One-Loop Tadpole

Similar to bubble graph, for the two-site one-loop tadpole graph, there are also two ways to divide the graph into two subgraphs composed by connected tubes:

$$\psi_{2,(a)}^{(1)\text{tad}} = \frac{1}{X_1+Y_1} \times \frac{1}{X_2+Y_1+2Y_2} \times \frac{1}{X_1+X_2+2Y_2} \times \frac{1}{X_1+X_2}, \quad (4.18a)$$

$$\psi_{2,(b)}^{(1)\text{tad}} = \frac{1}{X_1+Y_1} \times \frac{1}{X_2+Y_1+2Y_2} \times \frac{1}{X_2+Y_1} \times \frac{1}{X_1+X_2}, \quad (4.18b)$$

where each subgraph contains four tubes. Summing over the two contributions in Eq. (4.18), we can obtain the full wavefunction coefficient $\psi_{2,\text{Mink}}^{(1)\text{tad}}$ as computed in Eq. (3.36).

When the graphs are dressed with cross signs on their internal edges, they generate all the relevant letters associated with tubes, as summarized in Table. 2

l_1		$\text{dlog}(X_1 + Y_1)$	l_2		$\text{dlog}(X_2 + Y_1)$
l_3		$\text{dlog}(X_1 - Y_1)$	l_4		$\text{dlog}(X_2 - Y_1)$
l_5		$\text{dlog}(X_1 + X_2)$			
\bar{l}_2		$\text{dlog}(X_2 + Y_1 + 2Y_2)$	\bar{l}_4		$\text{dlog}(X_2 - Y_1 + 2Y_2)$
\bar{l}_5		$\text{dlog}(X_1 + X_2 + 2Y_2)$			

Table 2. The alphabet for two-site one-loop tadpole-type wavefunction coefficient, where the letters $l_i = \text{dlog}(w_i)$, $\bar{l}_j = \text{dlog}(\bar{w}_j)$ and $\{l_6, l_7\}$ are excluded.

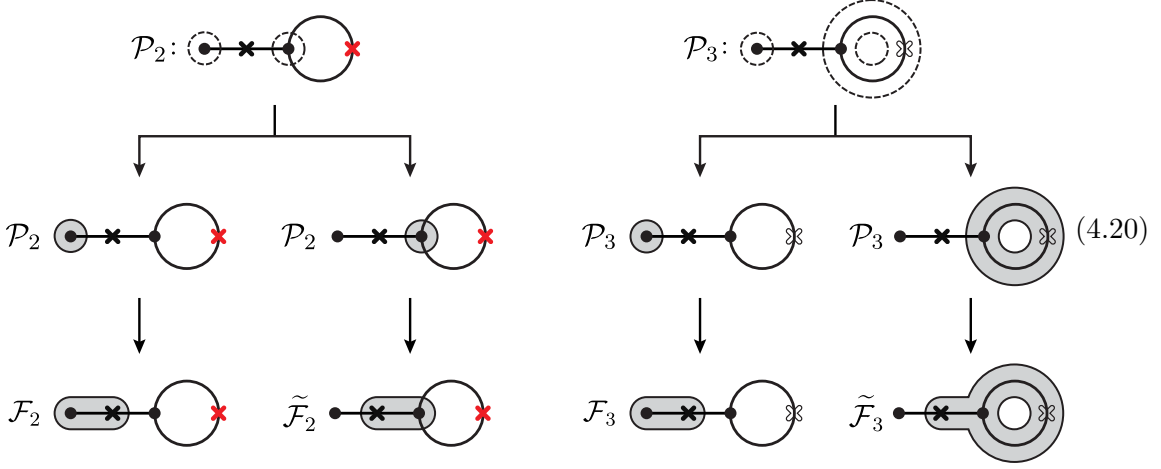
The eight physical functions within the integral family (3.55) can also be categorized into three layers. Each layer is characterized by its own set of associated tubing graphs, which provide a graphical representation. These tubing graphs are explicitly illustrated as follows:

Layer-0					
Layer-1	\mathcal{F}_2	$\tilde{\mathcal{F}}_2$	\mathcal{F}_3	$\tilde{\mathcal{F}}_3$	(4.19)
Layer-2	\mathcal{Q}_2	\mathcal{Q}_3			

where there are two distinct parent function \mathcal{P}_2 and \mathcal{P}_3 in layer-0 as discussed in Section 3.2. Further, for the functions $\{\mathcal{P}_2, \mathcal{F}_2, \tilde{\mathcal{F}}_2\}$, the red-marked cross signs indicate that these cross signs cannot be enclosed by the activated tube during the generation of the family tree. And for the functions $\{\mathcal{P}_3, \mathcal{F}_3, \tilde{\mathcal{F}}_3\}$, the hollow cross signs represent “ineffective” markers, meaning that tubes containing these hollow cross signs adhere to the same growth rules as those without any cross signs. Specifically, they will enclose their adjacent solid cross signs, as demonstrated below.

Now, let us analyze the kinematic flow structure of the function corresponding to the tadpole graph. First, for the layer-1 functions, there are two distinct parent functions \mathcal{P}_2

and \mathcal{P}_3 , each of them contains two seed tubes. These seed tubes can be activated and then enclose their adjacent cross signs, forming two distinct branches:



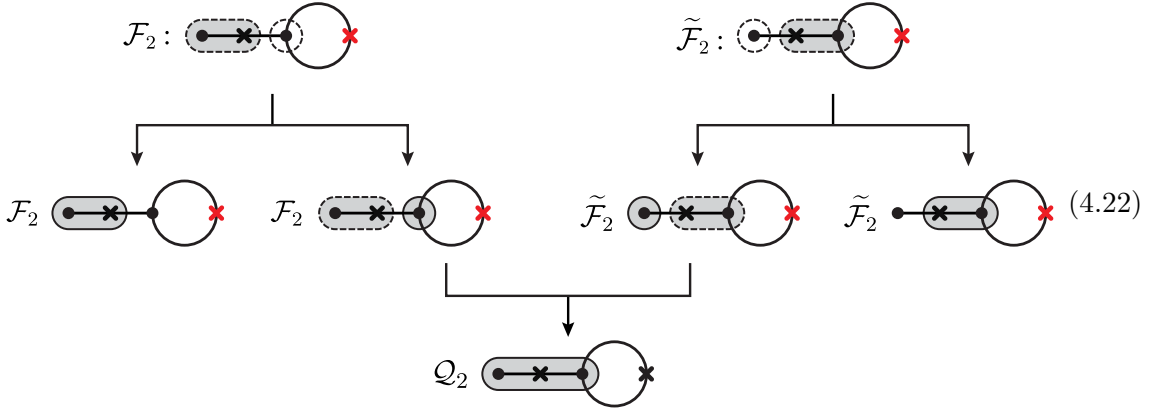
In the second branch of \mathcal{P}_2 , the activated tube can only enclose the black-marked cross sign; otherwise, the resulting graph would mix into the family tree of \mathcal{P}_3 . On the other hand, in the second branch of \mathcal{P}_3 , the presence of a hollow cross sign allows the activated tube to enclose one additional adjacent cross sign. Therefore, the canonical DEs are obtained according to the family trees (4.20)

$$\begin{aligned} d\mathcal{P}_2 &= \varepsilon [(\mathcal{P}_2 - \mathcal{F}_2)l_1 + (\mathcal{P}_2 - \tilde{\mathcal{F}}_2)\bar{l}_2 + \mathcal{F}_2l_3 + \tilde{\mathcal{F}}_2\bar{l}_4] \\ &= \varepsilon [\mathcal{P}_2(l_1 + \bar{l}_2) + \mathcal{F}_2(l_3 - l_1) + \tilde{\mathcal{F}}_2(\bar{l}_4 - \bar{l}_2)], \end{aligned} \quad (4.21a)$$

$$\begin{aligned} d\mathcal{P}_3 &= \varepsilon [(\mathcal{P}_3 - \mathcal{F}_3)l_1 + (\mathcal{P}_3 - \tilde{\mathcal{F}}_3)l_2 + \mathcal{F}_3l_3 + \tilde{\mathcal{F}}_3l_4] \\ &= \varepsilon [\mathcal{P}_3(l_1 + l_2) + \mathcal{F}_3(l_3 - l_1) + \tilde{\mathcal{F}}_3(l_4 - l_2)], \end{aligned} \quad (4.21b)$$

where the letters $\{l_i, \bar{l}_j\}$ are given in Table. 2. From this, we can observe that the types of letters associated with \mathcal{P}_2 and \mathcal{P}_3 are not entirely the same, as they contain \bar{l}_2 and l_2 respectively. This distinction prevents \mathcal{P}_2 and \mathcal{P}_3 from being merged into a single function unlike the bubble case, where all parent functions share the same set of letters.

Next, for the descendant functions \mathcal{F}_2 and $\tilde{\mathcal{F}}_2$ in layer-1, their corresponding family trees are given by

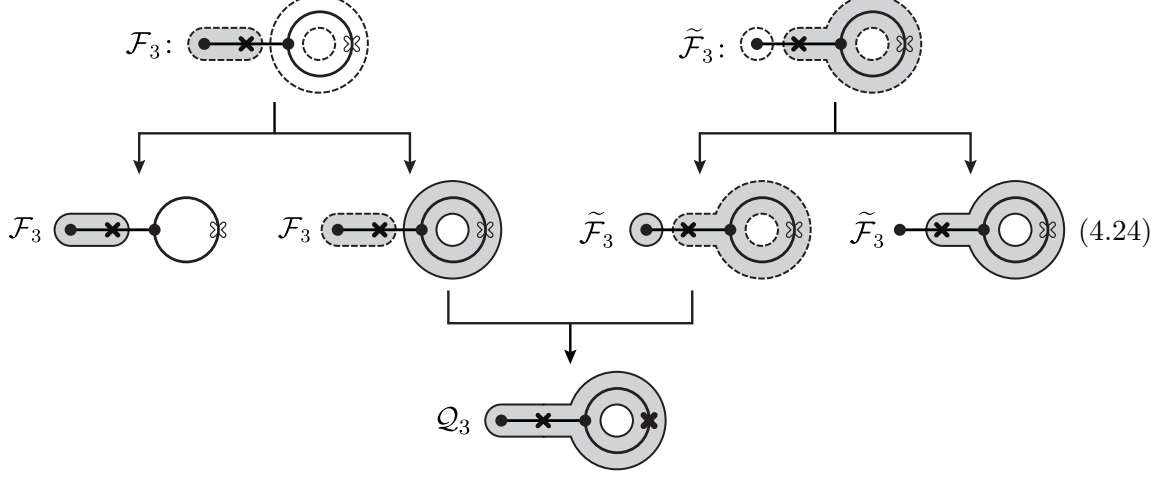


The corresponding canonical DEs can be obtained from the family trees (4.22) as follows:

$$d\mathcal{F}_2 = \varepsilon [(\mathcal{F}_2 - \mathcal{Q}_2)\bar{l}_2 + \mathcal{F}_2 l_3 + \mathcal{Q}_2 \bar{l}_5] = \varepsilon [\mathcal{F}_2(\bar{l}_2 + l_3) + \mathcal{Q}_2(\bar{l}_5 - \bar{l}_2)], \quad (4.23a)$$

$$d\tilde{\mathcal{F}}_2 = \varepsilon [(\tilde{\mathcal{F}}_2 - \mathcal{Q}_2)l_1 + \tilde{\mathcal{F}}_2 \bar{l}_4 + \mathcal{Q}_2 \bar{l}_5] = \varepsilon [\tilde{\mathcal{F}}_2(l_1 + \bar{l}_4) + \mathcal{Q}_2(\bar{l}_5 - l_1)]. \quad (4.23b)$$

Similarly, for the descendant functions \mathcal{F}_3 and $\tilde{\mathcal{F}}_3$ in layer-1, their corresponding family tree are given by

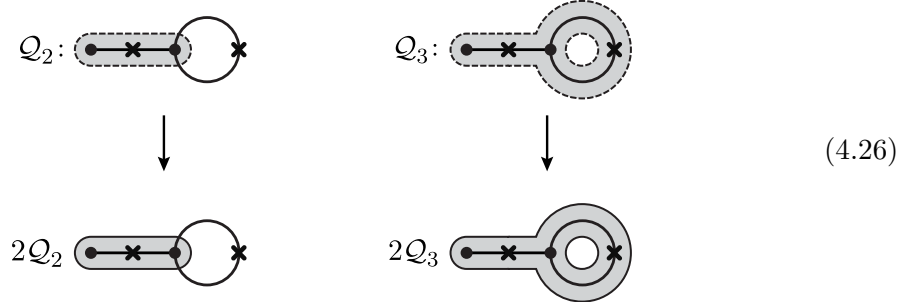


where the canonical DEs can be read from the Eq. (4.24) as follows:

$$d\mathcal{F}_3 = \varepsilon [(\mathcal{F}_3 - \mathcal{Q}_3)l_2 + \mathcal{F}_3 l_3 + \mathcal{Q}_3 l_5] = \varepsilon [\mathcal{F}_3(l_2 + l_3) + \mathcal{Q}_3(l_5 - l_2)], \quad (4.25a)$$

$$d\tilde{\mathcal{F}}_3 = \varepsilon [(\tilde{\mathcal{F}}_3 - \mathcal{Q}_3)l_1 + \tilde{\mathcal{F}}_3 l_4 + \mathcal{Q}_3 l_5] = \varepsilon [\tilde{\mathcal{F}}_3(l_1 + l_4) + \mathcal{Q}_3(l_5 - l_1)]. \quad (4.25b)$$

Finally, for the two descendant functions \mathcal{Q}_2 and \mathcal{Q}_3 in layer-2, each graph associated with them only contains a single tube which can be activated as:



where the canonical DEs can be obtained from the family tree (4.26) as follows:

$$d\mathcal{Q}_2 = 2\varepsilon \mathcal{Q}_2 \bar{l}_5, \quad d\mathcal{Q}_3 = 2\varepsilon \mathcal{Q}_3 l_5. \quad (4.27)$$

Finally, all the differential equations obtained from the family tree are found to be in complete agreement with the results derived in the previous chapter. This consistency not only validates the correctness of our approach but also highlights the robustness of the family tree method in systematically capturing the underlying structures of the equations. Further, it reinforces the broader applicability of this framework to more complex scenarios in future studies.

5 Conclusion and Outlook

In this study, we have systematically derived the canonical differential equations governing the two-site one-loop wavefunction coefficient within the framework of conformally-coupled scalar theory in general power-law FRW cosmologies. By employing the tools of relative twisted cohomology and integration-by-parts techniques, we propose an approach that combines the kinematic flow framework with the graphical representation of singularities through marked tubing graphs. This methodology represents a natural extension of the kinematic flow method from tree level to loop level, marking an important step forward in its development. Our study not only facilitates the derivation of differential equations but also provides a systematic and coherent graphical framework for studying loop-level correlators for the first time.

As we look to the future, our research will focus on extending these methodologies to the investigations for higher-loop and massive correlators. The extension of the kinematic flow framework to higher loops promises to unveil new mathematical structures that could further illuminate the intricate dynamics of cosmological models. Additionally, we also present a preliminary analysis of the differential equations associated with two-site two-loop sunset-type graphs in Appendix B and provide the general counting rules for arbitrary loop with two-site bubble-type graphs. Notably, all of these results represent the first implementation of the kinematic flow method at the loop level, highlighting its applicability to more intricate topologies. We are optimistic that this investigation will not only illuminate the intricate structures inherent in these graphs and serve as a catalyst for further advancements.

Acknowledgments

We are grateful to Paolo Benincasa, Giacomo Brunello, J. J. Carrasco, Zongzhe Du, Jianyu Gong, Xu Wang and Yu Wu for their insightful discussions and valuable suggestions. YH and CS would like to acknowledge the Northwestern University Amplitudes and Insight group, Department of Physics and Astronomy, and Weinberg College for support.

Appendix

A The Derivation of Two-Site One-Loop DEs from IBP

In this appendix, we provide additional details on the derivation of the differential equations for certain functions that were omitted in the main text.

A.1 Two-Site One-Loop Bubble

The total derivative for $\mathbf{F}_3 = \{\mathcal{P}_3, \mathcal{F}_3, \tilde{\mathcal{F}}_3, \mathcal{Q}_3\}$ is

$$d\mathbf{F}_3 = \partial_{X_1}\mathbf{F}_3 dX_1 + \partial_{X_2}\mathbf{F}_3 dX_2 + \partial_{Y_1}\mathbf{F}_3 dY_1 + \partial_{Y_2}\mathbf{F}_3 dY_2. \quad (\text{A.1})$$

The differentiation of external energy X_1 with respect to the parent function \mathcal{P}_3 can be calculated as follows:

$$\begin{aligned} \partial_{X_1}\mathcal{P}_3 &= \int d\mu \partial_{x_1} \bar{\Omega}_{\mathcal{P}_3}^2 = \varepsilon \int d\mu \left(-\frac{\bar{\Omega}_{\mathcal{P}_3}^2}{T_1} \right) \\ &= \varepsilon \int d\mu \left\{ \left(\text{Res} \left[\frac{-\bar{\Omega}_{\mathcal{P}_3}^2}{T_1} \right]_{\substack{L_1=0 \\ L_2=0}}, \text{Res} \left[\frac{-\bar{\Omega}_{\mathcal{P}_3}^2}{T_1} \right]_{\substack{T_1=0 \\ L_2=0}} \right) (\bar{\Omega}_{\mathcal{P}_3}^2, \bar{\Omega}_{\mathcal{F}_3}^2)^T \right\} \\ &= -\varepsilon \int d\mu \left[\frac{1}{X_1+Y_1+Y_2} \bar{\Omega}_{\mathcal{P}_3}^2 + \frac{2(Y_1+Y_2)}{(X_1-Y_1-Y_2)(X_1+Y_1+Y_2)} \bar{\Omega}_{\mathcal{F}_3}^2 \right] \\ &= -\varepsilon \left[\frac{1}{X_1+Y_1+Y_2} \mathcal{P}_3 + \left(\frac{1}{X_1-Y_1-Y_2} - \frac{1}{X_1+Y_1+Y_2} \right) \mathcal{F}_3 \right]. \end{aligned} \quad (\text{A.2})$$

Similarly, the differentiation with respect to X_2 follows the same steps as for X_1 , we only need to make the following substitutions: $X_1 \rightarrow X_2$ and $\mathcal{F}_3 \rightarrow \tilde{\mathcal{F}}_3$ in Eq. (A.2):

$$\partial_{X_2}\mathcal{P}_3 = \varepsilon \left[\frac{1}{X_2+Y_1+Y_2} \mathcal{P}_3 + \left(\frac{1}{X_2-Y_1-Y_2} - \frac{1}{X_2+Y_1+Y_2} \right) \tilde{\mathcal{F}}_3 \right]. \quad (\text{A.3})$$

The differentiation of internal energy Y_1 with respect to \mathcal{P}_3 can be computed as follows:

$$\begin{aligned} \partial_{Y_1}\mathcal{P}_3 &= \int d\mu \left[\partial_{x_1} \left(\frac{-x_1-X_1}{Y_1+Y_2} \bar{\Omega}_{\mathcal{P}_3}^2 \right) + \partial_{x_2} \left(\frac{-x_2-X_2}{Y_1+Y_2} \bar{\Omega}_{\mathcal{P}_3}^2 \right) \right] \\ &= \varepsilon \int d\mu \left\{ \left(\text{Res} \left[\frac{(x_1+X_1)\bar{\Omega}_{\mathcal{P}_3}^2}{T_1(Y_1+Y_2)} \right]_{\substack{L_1=0 \\ L_2=0}}, \text{Res} \left[\frac{(x_1+X_1)\bar{\Omega}_{\mathcal{P}_3}^2}{T_1(Y_1+Y_2)} \right]_{\substack{T_1=0 \\ L_2=0}} \right) (\bar{\Omega}_{\mathcal{P}_3}^2, \bar{\Omega}_{\mathcal{F}_3}^2)^T \right. \\ &\quad \left. + \left(\text{Res} \left[\frac{(x_1+X_1)\bar{\Omega}_{\mathcal{P}_3}^2}{T_2(Y_1+Y_2)} \right]_{\substack{L_1=0 \\ L_2=0}}, \text{Res} \left[\frac{(x_1+X_1)\bar{\Omega}_{\mathcal{P}_3}^2}{T_2(Y_1+Y_2)} \right]_{\substack{T_2=0 \\ L_1=0}} \right) (\bar{\Omega}_{\mathcal{P}_3}^2, \bar{\Omega}_{\tilde{\mathcal{F}}_3}^2)^T \right\} \\ &= \varepsilon \left[\left(\frac{1}{X_1+Y_1+Y_2} + \frac{1}{X_2+Y_1+Y_2} \right) \mathcal{P}_3 - \left(\frac{1}{X_1+Y_1+Y_2} + \frac{1}{X_1-Y_1-Y_2} \right) \mathcal{F}_3 \right. \\ &\quad \left. - \left(\frac{1}{X_2+Y_1+Y_2} + \frac{1}{X_2-Y_1-Y_2} \right) \tilde{\mathcal{F}}_3 \right]. \end{aligned} \quad (\text{A.4})$$

By replacing $Y_1 \rightarrow Y_2$ in Eq. (A.4), it is not difficult to derive the result for Y_2 :

$$\begin{aligned} \partial_{Y_2} \mathcal{P}_3 = \varepsilon \left[\left(\frac{1}{X_1+Y_1+Y_2} + \frac{1}{X_2+Y_1+Y_2} \right) \mathcal{P}_3 - \left(\frac{1}{X_1+Y_1+Y_2} + \frac{1}{X_1-Y_1-Y_2} \right) \mathcal{F}_3 \right. \\ \left. - \left(\frac{1}{X_2+Y_1+Y_2} + \frac{1}{X_2-Y_1-Y_2} \right) \tilde{\mathcal{F}}_3 \right] = \partial_{Y_1} \mathcal{P}_3. \end{aligned} \quad (\text{A.5})$$

Thus, in terms of the total derivative (A.1) and writing in dlog forms, we finally obtain the full differential equation for \mathcal{P}_3 :

$$\begin{aligned} d\mathcal{P}_3 = -\varepsilon \left[(\mathcal{P}_3 - \mathcal{F}_3) d\log(X_1+Y_1+Y_2) + (\mathcal{P}_3 - \tilde{\mathcal{F}}_3) d\log(X_2+Y_1+Y_2) \right. \\ \left. + \mathcal{F}_3 d\log(X_1-Y_1-Y_2) + \tilde{\mathcal{F}}_3 d\log(X_2-Y_1-Y_2) \right]. \end{aligned} \quad (\text{A.6})$$

Next, we examine the differentiation of the decedent functions \mathcal{F}_3 and $\tilde{\mathcal{F}}_3$. For \mathcal{F}_3 , the results with respect to the external energies is given by

$$\begin{aligned} \partial_{X_1} \mathcal{F}_3 &= \int d\mu \left[\partial_{x_1} \left(\frac{-T_1}{X_1-Y_1-Y_2} \bar{\Omega}_{\mathcal{F}_3}^2 \right) + \partial_{x_2} \left(\frac{-L_2}{X_1-Y_1-Y_2} \bar{\Omega}_{\mathcal{F}_3}^2 \right) \right] \\ &= \varepsilon \int d\mu \left\{ \left(\text{Res} \left[\frac{\bar{\Omega}_{\mathcal{F}_3}^2}{X_1-Y_1-Y_2} \right]_{\substack{T_1=0 \\ L_2=0}}, \text{Res} \left[\frac{\bar{\Omega}_{\mathcal{F}_3}^2}{X_1-Y_1-Y_2} \right]_{\substack{T_1=0 \\ T_2=0}} \right) (\bar{\Omega}_{\mathcal{F}_3}^2, \bar{\Omega}_{\mathcal{Q}_3}^2)^T \right. \\ &\quad \left. + \left(\text{Res} \left[\frac{L_2 \bar{\Omega}_{\mathcal{F}_3}^2}{T_2(X_1-Y_1-Y_2)} \right]_{\substack{T_1=0 \\ L_2=0}}, \text{Res} \left[\frac{L_2 \bar{\Omega}_{\mathcal{F}_3}^2}{T_2(X_1-Y_1-Y_2)} \right]_{\substack{T_1=0 \\ T_2=0}} \right) (\bar{\Omega}_{\mathcal{F}_3}^2, \bar{\Omega}_{\mathcal{Q}_3}^2)^T \right\} \\ &= \varepsilon \left[\frac{1}{X_1-Y_1-Y_2} \mathcal{F}_3 + \frac{1}{X_1+X_2} \mathcal{Q}_3 \right], \end{aligned} \quad (\text{A.7a})$$

$$\partial_{X_2} \mathcal{F}_3 = \int d\mu \partial_{x_2} \bar{\Omega}_{\mathcal{F}_3}^2 = \varepsilon \left[\frac{1}{X_2+Y_1+Y_2} \mathcal{F}_3 + \left(\frac{1}{X_1+X_2} - \frac{1}{X_2+Y_1+Y_2} \right) \mathcal{Q}_3 \right], \quad (\text{A.7b})$$

and the differentiation with respect to the internal energies is computed as:

$$\begin{aligned} \partial_{Y_1} \mathcal{F}_3 &= \int d\mu \left[\partial_{x_1} \left(\frac{x_1}{X_1-Y_1-Y_2} \bar{\Omega}_{\mathcal{F}_3}^2 \right) + \partial_{x_2} \left(\frac{x_2+X_1+X_2}{X_1-Y_1-Y_2} \bar{\Omega}_{\mathcal{F}_3}^2 \right) \right] \\ &= \varepsilon \left[\left(-\frac{1}{X_1-Y_1-Y_2} + \frac{1}{X_2+Y_1+Y_2} \right) \mathcal{F}_3 - \frac{1}{X_2+Y_1+Y_2} \mathcal{Q}_3 \right], \end{aligned} \quad (\text{A.8a})$$

$$\partial_{Y_2} \mathcal{F}_3 = \partial_{Y_1} \mathcal{F}_3. \quad (\text{A.8b})$$

We omit the derivation for $\tilde{\mathcal{F}}_3$. In terms of the total derivative, the complete canonical differential equations for \mathcal{F}_3 and $\tilde{\mathcal{F}}_3$ are obtained as:

$$d\mathcal{F}_3 = \varepsilon [\mathcal{F}_3 d\log(X_1-Y_1-Y_2) + (\mathcal{F}_3 - \mathcal{Q}_3) d\log(X_2+Y_1+Y_2) + \mathcal{Q}_3 d\log(X_1+X_2)], \quad (\text{A.9a})$$

$$d\tilde{\mathcal{F}}_3 = \varepsilon [\tilde{\mathcal{F}}_3 d\log(X_2-Y_1-Y_2) + (\tilde{\mathcal{F}}_3 - \mathcal{Q}_3) d\log(X_1+Y_1+Y_2) + \mathcal{Q}_3 d\log(X_1+X_2)]. \quad (\text{A.9b})$$

Finally, for the descendant function \mathcal{Q}_3 , we can derive

$$\partial_{X_1} \mathcal{Q}_3 = \int d\mu \left[\partial_{x_1} \left(\frac{-x_1}{X_1+X_2} \bar{\Omega}_{\mathcal{Q}_3}^2 \right) + \partial_{x_2} \left(\frac{-x_2}{X_1+X_2} \bar{\Omega}_{\mathcal{Q}_3}^2 \right) \right]$$

$$= 2\varepsilon \int d\mu \operatorname{Res} \left[\frac{\bar{\Omega}_{\mathcal{Q}_3}^2}{X_1 - X_2} \right]_{\substack{T_1=0 \\ T_2=0}} \bar{\Omega}_{\mathcal{Q}_3}^2 = 2\varepsilon \frac{\mathcal{Q}_3}{X_1 + X_2}, \quad (\text{A.10a})$$

$$\partial_{X_2} \mathcal{Q}_3 = \partial_{X_1} \mathcal{Q}_3, \quad (\text{A.10b})$$

$$\partial_{Y_1} \mathcal{Q}_3 = \partial_{Y_2} \mathcal{Q}_3 = 0, \quad (\text{A.10c})$$

where the differential equation for \mathcal{Q}_3 is obtained as:

$$d\mathcal{Q}_3 = 2\varepsilon \mathcal{Q}_3 d\log(X_1 + X_2). \quad (\text{A.11})$$

A.2 Two-Site One-Loop Tadpole

The differentiation for the function \mathcal{R}_2 with respect to the external and internal energies is computed as:

$$\begin{aligned} \partial_{X_1} \mathcal{R}_2 &= \int d\mu \left[\partial_{x_1} \left(\frac{-x_1}{X_1 - Y_1 + 2Y_2} \bar{\Omega}_{\mathcal{R}_2}^2 \right) + \partial_{x_2} \left(\frac{-L_2}{X_1 - Y_1 + 2Y_2} \bar{\Omega}_{\mathcal{R}_2}^2 \right) \right] \\ &= \varepsilon \left[\frac{1}{X_1 - Y_1 + 2Y_2} \mathcal{R}_2 + \frac{1}{X_1 + X_2 + 2Y_2} \mathcal{Q}_2 \right], \end{aligned} \quad (\text{A.12a})$$

$$\partial_{X_2} \mathcal{R}_2 = \int d\mu \partial_{x_2} \bar{\Omega}_{\mathcal{R}_2}^2 = \varepsilon \left[\frac{1}{X_2 + Y_1} \mathcal{R}_2 + \left(\frac{1}{X_1 + X_2 + 2Y_2} - \frac{1}{X_2 + Y_1} \right) \mathcal{Q}_2 \right], \quad (\text{A.12b})$$

$$\begin{aligned} \partial_{Y_1} \mathcal{R}_2 &= \int d\mu \left[\partial_{x_1} \left(\frac{x_1}{X_1 - Y_1 + 2Y_2} \bar{\Omega}_{\mathcal{R}_2}^2 \right) + \partial_{x_2} \left(\frac{x_2 + X_1 + X_2 + 2Y_2}{X_1 - Y_1 + 2Y_2} \bar{\Omega}_{\mathcal{R}_2}^2 \right) \right] \\ &= \varepsilon \left[\left(\frac{1}{X_2 + Y_1} - \frac{1}{X_1 - Y_1 + 2Y_2} \right) \mathcal{R}_2 - \frac{1}{X_2 + Y_1} \mathcal{Q}_2 \right], \end{aligned} \quad (\text{A.12c})$$

$$\begin{aligned} \partial_{Y_2} \mathcal{R}_2 &= \int d\mu \left[\partial_{x_1} \left(\frac{-2x_1}{X_1 - Y_1 + 2Y_2} \bar{\Omega}_{\mathcal{R}_2}^2 \right) + \partial_{x_2} \left(\frac{-2L_2}{X_1 - Y_1 + 2Y_2} \bar{\Omega}_{\mathcal{R}_2}^2 \right) \right] \\ &= \varepsilon \left[\frac{2}{X_1 - Y_1 + 2Y_2} \mathcal{R}_2 + \frac{2}{X_1 + X_2 + 2Y_2} \mathcal{Q}_2 \right]. \end{aligned} \quad (\text{A.12d})$$

Collectively, the canonical differential equation for \mathcal{R}_2 is

$$\begin{aligned} d\mathcal{R}_2 &= \varepsilon \left[\mathcal{R}_2 d\log(X_1 - Y_1 + 2Y_2) + (\mathcal{R}_2 - \mathcal{Q}_2) d\log(X_2 + Y_1) \right. \\ &\quad \left. + \mathcal{Q}_2 d\log(X_1 + X_2 + 2Y_2) \right]. \end{aligned} \quad (\text{A.13})$$

The differentiation for the function \mathcal{R}_3 with respect to the external and internal energies is computed as:

$$\begin{aligned} \partial_{X_1} \mathcal{R}_3 &= \int d\mu \left[\partial_{x_1} \left(\frac{-x_1}{X_1 - Y_1 - 2Y_2} \bar{\Omega}_{\mathcal{R}_3}^2 \right) + \partial_{x_2} \left(\frac{-x_2 - X_2 - Y_1 - 2Y_2}{X_1 - Y_1 - 2Y_2} \bar{\Omega}_{\mathcal{R}_3}^2 \right) \right] \\ &= \varepsilon \left[\frac{1}{X_1 - Y_1 - 2Y_2} \bar{\Omega}_{\mathcal{R}_3}^2 + \frac{1}{X_1 + X_2} \bar{\Omega}_{\mathcal{Q}_3}^2 \right], \end{aligned} \quad (\text{A.14a})$$

$$\begin{aligned} \partial_{X_2} \mathcal{R}_3 &= \int d\mu \partial_{x_2} \bar{\Omega}_{\mathcal{R}_3}^2 = \int d\mu \left(-\frac{\bar{\Omega}_{\mathcal{R}_3}^2}{T_2} \right) \\ &= \varepsilon \left[\frac{1}{X_2 + Y_1 + 2Y_2} \bar{\Omega}_{\mathcal{R}_3}^2 + \left(\frac{1}{X_1 + X_2} - \frac{1}{X_2 + Y_1 + 2Y_2} \right) \bar{\Omega}_{\mathcal{Q}_3}^2 \right], \end{aligned} \quad (\text{A.14b})$$

$$\begin{aligned}\partial_{Y_1} \mathcal{R}_3 &= \int d\mu \left[\partial_{x_1} \left(\frac{x_1}{X_1 - Y_1 - 2Y_2} \bar{\Omega}_{\mathcal{R}_3}^2 \right) + \partial_{x_2} \left(\frac{x_2 + X_1 + X_2}{X_1 - Y_1 - 2Y_2} \bar{\Omega}_{\mathcal{R}_3}^2 \right) \right] \\ &= \varepsilon \left[\left(\frac{1}{X_2 + Y_1 + 2Y_2} - \frac{1}{X_1 - Y_1 - 2Y_2} \right) \bar{\Omega}_{\mathcal{R}_3}^2 - \frac{1}{X_2 + Y_1 + 2Y_2} \bar{\Omega}_{\mathcal{Q}_3}^2 \right],\end{aligned}\quad (\text{A.14c})$$

$$\partial_{Y_2} \mathcal{R}_3 = 2\partial_{Y_1} \mathcal{R}_3. \quad (\text{A.14d})$$

Collectively, the canonical differential equation for \mathcal{R}_3 is

$$\begin{aligned}d\mathcal{R}_3 &= \varepsilon \left[\mathcal{R}_3 d\log(X_1 - Y_1 - 2Y_2) + (\mathcal{R}_3 - \mathcal{Q}_3) d\log(X_2 + Y_1 + 2Y_2) \right. \\ &\quad \left. + \mathcal{Q}_3 d\log(X_1 + X_2) \right].\end{aligned}\quad (\text{A.15})$$

B Analysis for Two-Site Higher Loop Graph

In this appendix, we generalize our method for two-site one-loop bubble diagram to higher loop order. We first study case of the two-site two-loop sunset-type wavefunction coefficient. The FRW wavefunction coefficient is computed as follows:

$$\begin{aligned}\psi_{2,\text{FRW}}^{(2)\text{sun}} &= -8Y_1 Y_2 Y_3 \int dx_1 \wedge dx_2 (T_1 T_2)^\varepsilon \\ &\quad \times \frac{1}{L_1 L_2 D_7} \left[\frac{1}{D_1} \left(\frac{1}{D_4} + \frac{1}{D_5} \right) + \frac{1}{D_2} \left(\frac{1}{D_4} + \frac{1}{D_6} \right) + \frac{1}{D_3} \left(\frac{1}{D_5} + \frac{1}{D_6} \right) \right] \\ &\equiv \int d\mu \bar{\Omega}_{\mathcal{P}}^2,\end{aligned}\quad (\text{B.1})$$

where the hyperplanes are defined as follows:

$$\begin{aligned}T_1 &= x_1, & T_2 &= x_2, \\ L_1 &= x_1 + X_1 + Y_1 + Y_2 + Y_3, & L_2 &= x_2 + X_2 + Y_1 + Y_2 + Y_3, \\ D_1 &= x_1 + x_2 + X_1 + X_2 + 2Y_1, & D_2 &= x_1 + x_2 + X_1 + X_2 + 2Y_2, \\ D_3 &= x_1 + x_2 + X_1 + X_2 + 2Y_3, & D_4 &= x_1 + x_2 + X_1 + X_2 + 2(Y_1 + Y_2),\end{aligned}$$

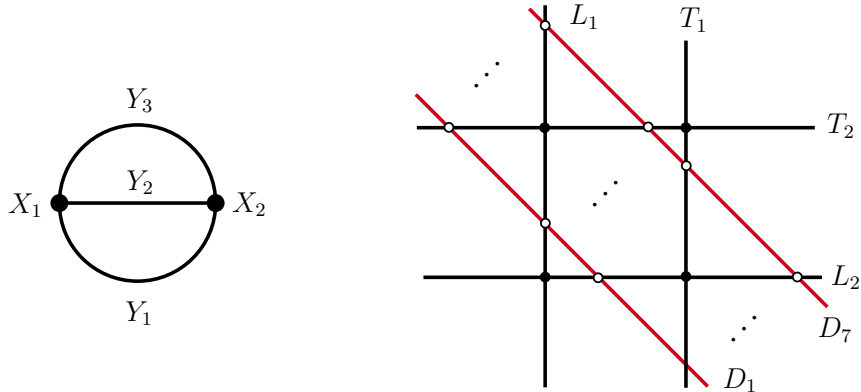


Figure 5. The Feynman diagram and hyperplane arrangement for the two-site two-loop sunset-type wavefunction coefficient.

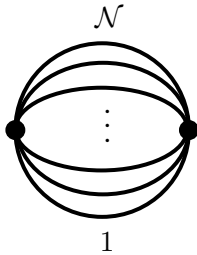


Figure 6. The Feynman diagram for the two-site L -loop bubble-type graph with N internal lines.

the number of loops, denoted by L , and the number of internal lines, $\mathcal{N} = L + 1$. For such an L -loop graph, we find that the number of independent functions can be expressed as:

$$1 + 2 \sum_{i=1}^{\mathcal{N}} \binom{\mathcal{N}}{i} + \sum_{i=1}^{\mathcal{N}} \binom{\mathcal{N}}{i} = 3 \cdot 2^{\mathcal{N}} - 2, \tag{B.6}$$

where N represents the number of internal lines in the graph. Additionally, the number of functions can be alternatively calculated as:

$$4S - (S - 1) = 3S + 1, \tag{B.7}$$

where S denotes the number of diagonally-placed hyperplanes $\{D_i\}$. The total number of letters is exactly one greater than the number of functions. We leave the investigation of more complex higher-loop cases for the future work.

l_1		$\text{dlog}(X_1+Y_1+Y_2+Y_3)$	l_2		$\text{dlog}(X_2+Y_1+Y_2+Y_3)$
l_3		$\text{dlog}(X_1+Y_1+Y_2-Y_3)$	l_4		$\text{dlog}(X_2+Y_1+Y_2-Y_3)$
l_5		$\text{dlog}(X_1+Y_1-Y_2+Y_3)$	l_6		$\text{dlog}(X_2+Y_1-Y_2+Y_3)$
l_7		$\text{dlog}(X_1-Y_1+Y_2+Y_3)$	l_8		$\text{dlog}(X_2-Y_1+Y_2+Y_3)$
l_9		$\text{dlog}(X_1+Y_1-Y_2-Y_3)$	l_{10}		$\text{dlog}(X_2+Y_1-Y_2-Y_3)$
l_{11}		$\text{dlog}(X_1-Y_1+Y_2-Y_3)$	l_{12}		$\text{dlog}(X_2-Y_1+Y_2-Y_3)$
l_{13}		$\text{dlog}(X_1-Y_1-Y_2+Y_3)$	l_{14}		$\text{dlog}(X_2-Y_1-Y_2+Y_3)$
l_{15}		$\text{dlog}(X_1-Y_1-Y_2-Y_3)$	l_{16}		$\text{dlog}(X_2-Y_1-Y_2-Y_3)$
l_{17}		$\text{dlog}(X_1+X_2+2Y_1+2Y_2)$	l_{18}		$\text{dlog}(X_1+X_2+2Y_1+2Y_3)$
l_{19}		$\text{dlog}(X_1+X_2+2Y_2+2Y_3)$	l_{20}		$\text{dlog}(X_1+X_2+2Y_1)$
l_{21}		$\text{dlog}(X_1+X_2+2Y_2)$	l_{22}		$\text{dlog}(X_1+X_2+2Y_3)$
l_{23}		$\text{dlog}(X_1+X_2)$			

Table 3. The alphabet for the two-site one-loop sunset-type wavefunction coefficient where $l_i = \text{dlog}(w_i)$.

References

- [1] N. Arkani-Hamed, P. Benincasa, and A. Postnikov, “Cosmological Polytopes and the Wavefunction of the Universe,” [arXiv:1709.02813](https://arxiv.org/abs/1709.02813) [[hep-th](#)].

- [2] N. Arkani-Hamed and P. Benincasa, “On the Emergence of Lorentz Invariance and Unitarity from the Scattering Facet of Cosmological Polytopes,” [arXiv:1811.01125 \[hep-th\]](#).
- [3] P. Benincasa, “From the flat-space S-matrix to the Wavefunction of the Universe,” [arXiv:1811.02515 \[hep-th\]](#).
- [4] P. Benincasa, “Cosmological Polytopes and the Wavefunction of the Universe for Light States,” [arXiv:1909.02517 \[hep-th\]](#).
- [5] S. De and A. Pokraka, “Cosmology meets cohomology,” *JHEP* **03** (2024) 156, [arXiv:2308.03753 \[hep-th\]](#).
- [6] P. Benincasa, G. Brunello, M. K. Mandal, P. Mastrolia, and F. Vazão, “On one-loop corrections to the Bunch-Davies wavefunction of the universe,” [arXiv:2408.16386 \[hep-th\]](#).
- [7] N. Arkani-Hamed, D. Baumann, A. Hillman, A. Joyce, H. Lee, and G. L. Pimentel, “Kinematic Flow and the Emergence of Time,” [arXiv:2312.05300 \[hep-th\]](#).
- [8] N. Arkani-Hamed, D. Baumann, A. Hillman, A. Joyce, H. Lee, and G. L. Pimentel, “Differential Equations for Cosmological Correlators,” [arXiv:2312.05303 \[hep-th\]](#).
- [9] K. Aomoto, “On vanishing of cohomology attached to certain many valued meromorphic functions,” *Journal of the Mathematical Society of Japan* **27** no. 2, (1975) 248–255.
- [10] K. Aomoto and M. Kita, *Theory of Hypergeometric Functions*. Springer Monographs in Mathematics. Springer, 2011.
- [11] P. Mastrolia and S. Mizera, “Feynman Integrals and Intersection Theory,” *JHEP* **02** (2019) 139, [arXiv:1810.03818 \[hep-th\]](#).
- [12] J. M. Henn, “Multiloop integrals in dimensional regularization made simple,” *Phys. Rev. Lett.* **110** (2013) 251601, [arXiv:1304.1806 \[hep-th\]](#).
- [13] J. M. Henn, “Lectures on differential equations for Feynman integrals,” *J. Phys. A* **48** (2015) 153001, [arXiv:1412.2296 \[hep-ph\]](#).
- [14] M. Carr and S. L. Devadoss, “Coxeter complexes and graph-associahedra,” *Topology and its Applications* **153** no. 12, (2006) 2155–2168.
- [15] S. L. Devadoss and M. Smith, “Colorful graph associahedra,” [arXiv:2011.08169](#).
- [16] P.-H. Balduf, A. Cantwell, K. Ebrahimi-Fard, L. Nabergall, N. Olson-Harris, and K. Yeats, “Tubings, chord diagrams, and dyson–schwinger equations,” *Journal of the London Mathematical Society* **110** no. 5, (2024) e70006.
- [17] N. Arkani-Hamed, Y. Bai, and T. Lam, “Positive Geometries and Canonical Forms,” *JHEP* **11** (2017) 039, [arXiv:1703.04541 \[hep-th\]](#).
- [18] A. B. Goncharov, M. Spradlin, C. Vergu, and A. Volovich, “Classical Polylogarithms for Amplitudes and Wilson Loops,” *Phys. Rev. Lett.* **105** (2010) 151605, [arXiv:1006.5703 \[hep-th\]](#).
- [19] C. Duhr, H. Gangl, and J. R. Rhodes, “From polygons and symbols to polylogarithmic functions,” *JHEP* **10** (2012) 075, [arXiv:1110.0458 \[math-ph\]](#).
- [20] C. Duhr and F. Dulat, “PolyLogTools — polylogs for the masses,” *JHEP* **08** (2019) 135, [arXiv:1904.07279 \[hep-th\]](#).
- [21] A. Hillman, “Symbol Recursion for the dS Wave Function,” [arXiv:1912.09450 \[hep-th\]](#).